

ResearchOnline@JCU

This file is part of the following reference:

Davis, Toby Patrick (2004) *Structural controls on Zn-Pb-Ag mineralisation determined by scale integrated analysis at Mount Isa, Queensland, Australia*. PhD thesis, James Cook University.

Access to this file is available from:

<http://eprints.jcu.edu.au/24945/>

If you believe that this work constitutes a copyright infringement, please contact ResearchOnline@jcu.edu.au and quote <http://eprints.jcu.edu.au/24945/>

Part D

Textural and microstructural analysis of the Zn-Pb-Ag and copper ores at Mount Isa

Textural and microstructural analysis of the Zn-Pb-Ag and copper ores at Mount Isa

Abstract	D-1
Introduction	D-2
Geological Background	D-3
Ore Textures	D-5
<i>Microcrystalline pyrite bands</i>	D-6
<i>Microcrystalline sphalerite bands</i>	D-6
<i>Fine grained sphalerite bands and microbreccias</i>	D-8
<i>Galena bands</i>	D-9
<i>'Nodular' layers</i>	D-9
<i>Zn-Pb-Ag breccias</i>	D-9
<i>Copper breccias</i>	D-12
<i>Discordant veins</i>	D-12
<i>Transitional zones</i>	D-13
Distribution of the ore textures	D-13
Microstructures	D-14
<i>'Nodular' layers</i>	D-14
<i>Microcrystalline pyrite</i>	D-14
<i>Microcrystalline sphalerite</i>	D-15
<i>Fine grained sphalerite</i>	D-15
<i>Galena bands</i>	D-16
<i>Foliation fill breccias</i>	D-16
<i>Fold clast breccias</i>	D-16
<i>Rounded clast breccias</i>	D-17
<i>Asymmetric boudin breccias</i>	D-17
Discussion	D-17
Conclusions	D-23
Acknowledgements	D-25
Tables	D-26
Figures	D-27 – D-60

Abstract

The Mount Isa Zn-Pb-Ag orebody consists of conformable sulphide bands and breccias whose enveloping surfaces are parallel to layering at hand specimen and exposure-scales. The range of textural variation in the bands and breccias and their distribution has been determined by logging drill core throughout the orebody. The deposit is zoned with respect to ore textures and it contains a core of breccias surrounded by sulphide band textural styles. All ore textural styles have NNW-SSE-striking trends, which is the same orientation as fold-hosted mine-scale high-grade shoots. All sulphide band and breccia textural variants exhibit a similar paragenetic sequence indicating that they formed at similar times. There are no overprinting relationships indicating remobilisation occurred within the deposit. Microstructural examination of each band and breccia style using oriented samples shows that all sulphide deposition was structurally controlled and the kinematics of processes involved in orebody development. Localisation of shearing strain throughout the deformation history played an important role in the formation of the host structures to the sulphides. It produced heterogeneities at a range of scales that were vital for dilation during mineralisation. Dilation occurred to accommodate differential progressive deformation between adjacent volumes. Localisation between competency domains defined by rock type led to mineralisation being limited to some specific beds or zones and ultimately producing stratiform style ores. Higher strains occurred in shaly rock types compared to siltstones and mudstones and produced the bedding parallel sulphide textures that are commonly misinterpreted to represent predeformation mineralisation. The difference in scale of deformation partitioning between the copper and Zn-Pb-Ag orebodies could explain the separation of metals between the two orebodies. Such a difference in the scale of structures hosting ore minerals would produce a sharp contrast in the fluid/rock ratio between the ore bodies, which would ultimately influencing the chemical environment. Consequently, copper was deposited within the silica-dolomite bodies but lead and zinc were permitted to pass beyond it before being deposited.

Introduction

More than half of the global reserves of lead and zinc are contained within stratiform sediment hosted Zn-Pb-Ag deposits meaning they are the world's most important source of these metals (Goodfellow et al. 1993; Large et al. 2002). The Mount Isa deposit occurs in the Carpentaria Zinc Belt of northern Australia, which contains five of the world's ten largest sediment-hosted Zn-Pb-Ag deposits making it one of the most significant base metal districts on Earth. This deposit is unique among the Zn-Pb-Ag deposits in the Carpentaria Zinc Belt because it contains large syntectonic copper orebodies adjacent to stratiform sediment hosted Zn-Pb-Ag ores. The latter deposit class is characterised by bedding-parallel sulphide concentrations at meso-scales that have been widely interpreted to be diagnostic of pre-deformation mineralisation (Neudert 1986; Forrestal, 1990; Valenta, 1994; Large et al 1998, 2002; Chapman, 2004). As a result, the copper and Zn-Pb-Ag mineralisation have been considered to have formed at different times (Perkins 1984; McGoldrick and Large, 1998; Waring et al., 1998).

Perkins (1997) showed that syntectonic sulphide deposition has occurred in the Mount Isa Zn-Pb-Ag orebody, but the extent to which this is representative of the entire deposit was unclear. This led later workers to suggest that the features presented by Perkins (1997) were the result of remobilization of a pre-tectonic deposit (Large et al., 1998; Marshall and Spry, 2000; Betts and Lister, 2002). Consequently, the role of Isan Orogeny (1620-1500 Ma) structures in the formation of this orebody has remained ambiguous. A recent study by Davis (2004; Part A) examined the relationship between mine-scale metal distribution and structures in the Zn-Pb-Ag and copper orebodies at Mount Isa. A ubiquitous correlation between the zinc and lead distribution and Isan Orogeny structures was found. Orebody geometries and relationships between metal distribution and tectonic structures are similar in the Zn-Pb-Ag and copper orebodies. Furthermore, it was found that, if the formation of the present orebodies was related to remobilisation of a pre-deformation deposit, then the older accumulation was not located in the vicinity of the Mount Isa deposit. Therefore, all the Zn-Pb-Ag mineralisation is most likely to be syntectonic in origin.

This study is part of a scale-integrated structural analysis of the Mount Isa Zn-Pb-Ag orebody. The aim was to investigate the textural features of the ores and their distribution in order to determine the extent of structurally controlled sulphide deposition and the kinematic processes involved in developing it in order to resolve the timing of mineralisation. The distribution of ore textures was determined by detailed logging of drill core, and orientated samples were used to examine microstructural and textural features of each ore textural style.

Samples from the nearby copper orebodies were also examined and compared to the Zn-Pb-Ag ores to determine whether there is any relationships between the two.

Geological Background

The Mount Isa Inlier, in western Queensland, Australia (Fig. 1), is divided into meridional belts by major N-S-striking faults (Blake and Stewart, 1992). Mount Isa is located on the western edge of the Leichhardt River Fault Trough, which is a subdivision of the Western Fold Belt. The inlier is recognised as comprising two tectonostratigraphic sequences with the Zn-Pb-Ag deposits being located in the younger of these. The older sequence was metamorphosed and deformed during the Barramundi Orogeny (1900-1870 Ma). The other was deposited around the late Palaeoproterozoic to early Mesoproterozoic and deformed during the Isan Orogeny (1620-1500 Ma). There are two distinct phases to the Isan Orogeny (Bell, 1983; Bell and Hickey, 1998). Overall N-S shortening orogenesis was followed by a E-W shortening phase with individual horizontal compressional events separated by vertical compression deformations (Bell and Hickey, 1998; Mares, 1998; Adshead-Bell, 2000; Part B). Bell and Hickey (1998) attributed this style of deformation to cycles of crustal thickening during horizontal compression followed by gravitational collapse of the thickened crust.

Six deformations attributed to the Isan Orogeny are recognised at Mount Isa (Part B). The first (D_1) formed folds with E-W-striking axial planes during N-S shortening. This was followed by E-W shortening in D_2 that produced upright folds with a vertical N-S-striking axial planar cleavage. D_3 is the oldest recognised horizontal cleavage forming deformation in this study area. S_3 shows predominantly top to the east displacement. D_4 produced a NNW-SSE-striking vertical cleavage and folds. D_5 and D_6 produced subtly developed structures and tend to be localised into the hinges and short limbs of F_4 folds. They are most readily recognised by deformation of S_4 , which was initially rotated to a west-dipping attitude by vertical shortening in D_5 , and then a vertical orientation by east block up shearing along vertical S_6 (Part B).

The Mount Isa base metal deposit consists of spatially separate copper (255 Mt at 3.3 % Cu) and Zn-Pb-Ag orebodies (150 Mt at 7 % Zn, 6% Pb and 150 g/t Ag) (Fig. 1; Part A). The copper orebodies comprise chalcopyrite-bearing breccias in a quartz-dolomite alteration body. The Zn-Pb-Ag ores comprise sulphide bands and breccias that are conformable to bedding at exposure-scales. The deposit is hosted by the Urquhart Shale, which belongs to the upper Mount Isa Group, and includes carbonaceous shales, massive siltstones and mudstones, and aphanitic K-feldspar dominant tuffaceous beds. These latter beds are used for stratigraphic correlation. Neudert (1986) listed the main rock types as massive siltstone, laminated siltstone,

discontinuously laminated siltstone, mudstone and carbonaceous mudstone, feldspathic chert, silty carbonate and nodular carbonate. Bell et al. (1988) subdivided the Urquhart Shale into three rock types based on the ratio of dolomite to mica plus carbonaceous material. These were, 1) black shale; containing less than 25 percent dolomite, 2) dolomitic shale; comprising 25-75 percent dolomite, and 3) dolomitic siltstone; with more than 75 percent dolomite.

Carbonaceous shales have a laminated appearance and contain ferroan-carbonate (ferroan-dolomite to ankerite), quartz and seams of graphite, pyrite and phyllosilicates. Bands and nodules of neoform ferroan carbonate, calcite and quartz as well as carbonaceous seams impart a laminated appearance to the shales (Fig. 2). The carbonaceous shales correspond to the laminated siltstones described by Neudert (1986) and the black shale and dolomitic shale of Bell et al. (1988).

Massive siltstones and mudstones are either thinly (<2 cm) or thick-bedded (>2 cm) and are most abundant between the ore packages. They also comprise a significant component of the ore packages where they separate individual sulphide bands and are present as clasts in breccias. Siltstones and mudstones consist of near monomineralic mosaic textured ferroan carbonate with traces of quartz. They generally lack carbonaceous seams though faint cleavage seams are occasionally observed (Fig. 2).

There are ten Zn-Pb-Ag lenses at the mine-scale, which are broadly conformable bodies that may contain numerous ore packages (Fig. 3). These were defined in Part A from a modelled plan of Pb+Zn through level 12 of the mine and are labelled B-K. Ore packages consist of centimetre- to decimetre-scale conformable sulphide bands and breccias interlayered with massive siltstone and mudstone beds. Groupings of these packages correspond to 'orebodies' defined at the mine-scale and used by other workers (e.g. Perkins, 1997). Using detailed stratigraphic correlation Perkins (1997) was able to demonstrate that the 'orebodies' transgress stratigraphy, although they may appear to be conformable by observation of a single level plan. The ore packages are separated by barren siltstone units that are several metres thick, but are generally too closely spaced to be individually recognised on mine-scale plans of metal distribution. In this study the term orebody refers collectively to all the Zn-Pb-Ag lenses in the deposit.

The distribution of the sulphide textures was examined across lens K which consists of five ore packages east of the 1380 orebody (Fig. 3). This lens was studied because it has the most comprehensive coverage of available drill core. It is also located on the eastern side of the mine making it the most distal Zn-Pb-Ag lens to the main centres of copper mineralisation. This latter feature meant that, if Zn-Pb-Ag ores pre-dated the copper ones, it had the highest

likelihood of being least affected by the later mineralisation event, and thereby the highest probability of preserving primary textures.

The southern margin of lens K corresponds to silica-dolomite alteration that is linked to copper mineralisation (Fig. 3). In longitudinal projections, lens K consists of a single NNW-plunging high grade shoot with an asymmetric grade distribution in which the highest grades are located closest to the southern end, next to the silica-dolomite alteration front (Fig. 3). A series of holes covering the area from within the silica-dolomite alteration to the northern periphery of the Zn-Pb-Ag orebody were examined. Barren intervals of thin-bedded siltstones interbedded with lesser thick-bedded siltstones (>2 cm) between the Zn-Pb-Ag packages are between 2 and 2.5m wide and rarely contain non-siltstone rock types. Individual Zn-Pb-Ag ore packages are 0.7 to 5 m wide and are continuous with stratiform protrusions of silica-dolomite alteration or microcrystalline pyrite-altered horizons. Intercalated siltstones comprise an average of 41.6% of the ore packages and are dominantly thick-bedded.

Ore Textures

The conformable nature of the sulphide bands and breccias is scale dependent. At hand specimen-scale the bands have the appearance of being conformable to layering and near monomineralic, comprising either sphalerite or pyrite and rarely galena. However, at micro-scales these bands contain significant amounts of remnant host rock with sulphides and associated alteration gangue minerals hosted in bedding discordant structures and. Individual breccias are conformable because they are situated between layers that are substantially unfolded. Layering within the breccias is deformed and cut by veins containing sulphides. The bulk of the galena in the deposit and a significant amount of the sphalerite is contained in such breccias. Bedding discordant veins, proximal to the ores but not included in the breccias, host an extremely small amount of ore minerals but are a significant part of the alteration that preceded mineralisation.

Sulphide bands are subdivided according to the dominant sulphide and grain size, into microcrystalline pyrite bands, microcrystalline sphalerite bands, fine grained sphalerite bands, and galena bands. Breccias are divided firstly into microbreccias and other breccias, which are subdivided based on the brecciation pattern. These are fold clast breccias, near massive fill breccias and planar fracture breccias. The latter consists of foliation fill breccias and asymmetric boudin breccias defined by the structural location of ore minerals.

Microcrystalline pyrite bands

'Microcrystalline' describes grainsizes in which individual grains cannot be discerned by the naked eye, whereas fine-grained ones are. Microcrystalline better describes the finest grained pyrite than the latter term which is used in previous works (e.g. Perkins, 1997; Perkins, 1998; Painter et al., 1999). Microcrystalline pyrite bands contain 70-90 % pyrite with a grainsize between 5-20 μm . Pyrite is arranged in anastomosing seams up to several grains wide that also contain accessory phyllosilicates and graphite (Fig. 4). Individual bands range from less than a millimetre to more than several tens of centimetres wide and are separated by massive siltstones or mudstones. The anastomosing seams are separated by sedimentary (pre metasomatic?) host rock carbonate (ferroan-dolomite) or neocrystalline carbonate (ferroan dolomite or calcite), quartz and pyrrhotite. The anastomosing fabric results from pyrite deposition along crenulated and crenulation cleavages. Pyrite has a spheroidal or euhedral habit with the former situated in a mosaic of 15-25 μm grain size carbonate. Euhedral pyrite is commonly associated with $\sim 40 \mu\text{m}$ sparry carbonate and quartz. Sphalerite and galena may be interstitial to pyrite aggregates or may occur in trace abundances in the domains between the anastomosing seams.

Microcrystalline sphalerite bands

Conformable sphalerite bands are a major part of the Zn-Pb-Ag orebody and account for 52.1 % of the combined thickness of base metal sulphide bands and breccias. They comprise sp-cte-fe dol-qz-po-py \pm chl \pm gn \pm cp in variable proportions and textures. Microcrystalline sphalerite ore styles have the least amount of accompanying alteration minerals of all sulphide textural styles in the Zn-Pb-Ag orebody. Sphalerite bands can be grouped into those comprising microcrystalline (5-40 μm) or dominantly fine grained sphalerite (10-300 μm).

Microcrystalline sphalerite bands have a massive or laminated appearance in hand specimen. The massive looking bands are pink and usually less than a centimetre wide (Fig. 5). These bands are the least important in terms of volume and only a few occurrences were observed in the diamond drill holes studied. Sphalerite typically comprises more than 50% of the rock and is arranged in a network of east-dipping or west-dipping 15-80 μm wide elongate and compact aggregates in 5-10 mm wide massive siltstone or mudstone beds (Fig. 5). Aggregates contain inclusions of ankerite or ferroan dolomite, quartz and pyrrhotite and are separated by either carbonate or quartz. The abundance of alteration related quartz and carbonate is proportional to the overall abundance of sphalerite in the rock. Pyrrhotite also forms elongate aggregates with the same orientation as sphalerite ones (Figs 5 c and d).

Laminated microcrystalline sphalerite bands have a fabric similar to the carbonaceous shales and comprise the bulk of microcrystalline sphalerite bands and 34.4 % of all base metal sulphide ore texture types by volume (Fig. 6). They have an average width of 5.9 cm and contain between 20-50 % sulphides of which sphalerite is the most abundant phase, with minor pyrrhotite, and accessory galena, pyrite and chalcopyrite. The shaly host rock has an uneven grainsize distribution compared to the mudstones that host the pink bands already mentioned. The laminated appearance is imparted by 40-80 μm elongated aggregates of sphalerite and anastomosing opaque seams similar to those in the carbonaceous shales. The opaque seams comprise spheroidal pyrite (5-20 μm) frequently replaced by galena or sphalerite. Sphalerite is most regularly situated between the opaque seams replacing carbonate, but also overprints them. Large euhedral pyrite grains with sphalerite and pyrrhotite inclusions and fibrous quartz beards are sporadically distributed throughout the laminated microcrystalline sphalerite bands.

Sphalerite is anhedral to euhedral with a tendency to idiomorphic grain shapes with increasing abundance. Lamellar twinning and individual grain boundaries are revealed by etching with hydriodic acid, and shows the grains are between 5-40 μm in size and that twins are largely undeformed and there is generally no lattice preferred orientation (Fig. 7). Mutual grain boundaries with other sphalerite or pyrrhotite grains are smooth and slightly curved but those with carbonate or quartz are complicated. These grain boundary relationships are not restricted to the microcrystalline sphalerite varieties, but are present wherever sphalerite and carbonate or quartz occur together. Pyrite is commonly present along sphalerite grain boundaries as elongated anhedral grains several microns wide (Fig. 7). Mineral inclusions in sphalerite grains are rare because of its small grainsize but where present are most commonly carbonate.

Pyrrhotite is situated in either aggregates up to 100 μm , or individual euhedral lath shaped grains up to, and occasionally greater than, 200 μm long (Fig. 7). Grain in the aggregates anhedral to subhedral grain shapes. Pyrrhotite is generally located in contact with sphalerite and displays the same shape preferred orientation as the surrounding sphalerite aggregates. Boundaries with quartz or carbonate are irregular. Galena and chalcopyrite are accessory phases in the massive microcrystalline sphalerite textural styles. They have grainsizes between 5-15 μm and are generally located together (Fig. 7). Galena and chalcopyrite are distributed either along the sphalerite grain boundaries or close to discordant qz-cb \pm chl veins.

Alteration-style quartz in the microcrystalline sphalerite ore textural styles is minor. Grains are subhedral to euhedral and between 5-15 μm in diameter, which is similar to the host rock carbonate (Fig. 7). Prismatic terminations are common and produce complex boundary shapes with sphalerite and pyrrhotite (Fig. 7). Aggregates and individual grains mainly occur as

older inclusions in sphalerite aggregates and within coarser grained carbonate. Quartz has weakly undulose extinction and is inclusion free. Carbonate adjacent to sphalerite is coarser than the host rock carbonate further away (Fig. 7). Euhedral crystals up to 200 μm may be zoned. The cores have straight extinction and the rims contain fine crystals (5-10 μm) of either carbonate or quartz (Fig. 7). Carbonate grains commonly contain sphalerite and other sulphide inclusions along crystallographic cleavage planes.

Fine grained sphalerite bands and microbreccias

Bands and microbreccias form end members in a spectrum of layer disruption in an ore textural style characterised by fine grained sphalerite. This style contains coarser sphalerite and more quartz and carbonate alteration relative to sulphides, compared with microcrystalline bands (Fig. 8). Fine grained sphalerite bands and microbreccias have an average thickness of 4.3 cm, contain sp-cte-fe dol-qz-py-po \pm cp \pm gn and account for 17.7 % of the Zn-Pb-Ag ores by volume. Bedding is least disrupted in the bands, whereas microbreccias contain vein and wall rock clasts as included folded layers up to several millimetres wide (Fig. 8). Folds are readily recognised in exposure samples but are more difficult to identify in drill core.

Sphalerite is distributed, on a micro-scale, in elongated aggregates with the same orientations as tectonic cleavages (Figs 8 a and b). It is subhedral to anhedral, between 10-300 μm , and comprises 20 to 30 % of the bands (Fig.9). Where sulphide concentration is low sphalerite is located along carbonate grain boundaries (Fig. 10). Grain boundary relationships are the same as in the microcrystalline sphalerite varieties. The orientation of laminar twinning indicates that fine grained sphalerite has random lattice orientations and there are two spatially separate grainsize populations (Fig. 9). One is 10-40 μm (microcrystalline) sphalerite grains in altered host rock inclusions within the bands. The other is 50-300 μm grains replacing carbonate in sites of dilation around the included layers.

Two generations of carbonate alteration preceded sphalerite mineralisation in the fine grained sphalerite textural style. The first was ferroan-carbonate (ferroan-dolomite to ankerite) with a murky appearance in plane polarised light and is commonly the main carbonate component in the east-dipping veins (Fig. 10). The other is calcite accompanied by quartz in veins that cut or replace ferroan carbonate veins (Fig. 11).

Quartz is subhedral to euhedral and ranges from several microns up to 300 μm and is a major phase in the fine grained sphalerite bands and microbreccias (Fig. 10). It is distributed randomly throughout these bands and microbreccias in aggregates up to several millimetres containing subhedral grains, occasionally with a fibrous habit. Mutual boundaries with other quartz grains are simple and those with carbonate or sulphide grains are more irregular (Fig.

9b). Disseminated euhedral pyrite, which is the youngest sulphide, has beards of fibrous quartz, indicating its deposition spanned base metal mineralisation (Fig. 6).

The fine grained sphalerite bands contain two texturally distinctive generations of pyrite. The oldest is the microcrystalline pyrite, which is disseminated or aggregated in patches of altered host rock clasts included in sphalerite aggregates (Fig. 10). The youngest pyrite consists of disseminated euhedral grains between 200 µm to several millimetres commonly associated with quartz (Fig.6). It overgrows the microcrystalline pyrite and locally contains sphalerite, pyrrhotite, galena and chalcopyrite inclusions because it is the most recently deposited sulphide.

Irregularly shaped pyrrhotite patches are intergrown with sphalerite, overprint S_4 and contain inclusions of the finest pyrite. Galena is a minor phase situated between sphalerite grains and in discordant veins. It is slightly more abundant in the fine grained sphalerite bands than in the microcrystalline ones. Chalcopyrite is an accessory sulphide that commonly accompanies galena. It occurs as 1-5 µm anhedral grains along sphalerite grain boundaries.

Galena bands

Conformable galena bands are rare, only two were encountered during this study in which 1266 individual conformable sulphide bands and breccias were measured. These bands have a fabric of anastomosing galena seams similar to the pyritic shales (Fig. 12). In Figure 12 the galena alteration front is situated behind a sphalerite ones with both sulphides replacing an unknown opaque phase. Galena in these bands also replaces fine grained spheroidal pyrite grains.

'Nodular' layers

Thin, bedding-parallel, nodular-looking layers up to several millimetres wide are a minor component of the ores. They consists of trails of porphyroblasts comprising ferroan dolomite and calcite with fine grained sphalerite inclusions (Fig. 13). The so-called nodular layers are commonly located near other base metal bands or breccias. Ferroan dolomite is dominantly located between the porphyroblasts whereas calcite is situated within them.

Zn-Pb-Ag breccias

Breccias, not including the fine grained sphalerite microbreccias, account for 36.5 % of stratabound sulphide textural styles in the Zn-Pb-Ag orebody at Mount Isa. Three styles of breccias based on fill and clast patterns were recognised (Figs. 14, 15, 16 and 17). (1) Planar fracture breccias are where dismemberment of the rock has occurred along planar structures. (2)

Fold clast breccias are characterised by clasts of folded layering. (3) Rounded clast breccias are dominated by the matrix and contain millimetre sized rounded clasts. All these patterns of brecciation may be contained within a single brecciated unit between intact and usually unfolded siltstone or mudstones layers (Fig. 16c). Breccias contain galena and sphalerite but are the host for the bulk of the former sulphide. The relative abundance of ore minerals varies between sphalerite or galena dominant end members. The average width of breccias measured in drill core is 7.3 cm but in underground exposures they can be greater than ten metres wide, containing numerous narrower breccias similar to those observed in drill core.

In planar fracture breccias, bedding is dismembered along moderate to steeply east- or west-dipping planar discontinuities at a high angle to S_0 that correspond to S_2 or S_3 cleavages. These breccias are clast dominated and there are two types that form depending on the relative strength of the interlayered rock types included in the breccia. Asymmetric boudin clast breccias formed where a high competency contrast existed between alternating layers. These typically consist of massive mudstone or siltstone, as competent layers, and carbonaceous shales, which are the least competent rock type (Fig. 15). Trains of siltstone asymmetric boudin clasts are separated by microcrystalline pyrite and sphalerite mineralised carbonaceous shale layers. Interboudin planes follow disjunctive S_2 with east block up displacement. Clast size reflects bedding thickness and the spacing of the disjunctive cleavages in the massive siltstones and mudstones.

Asymmetric boudin breccias are a sphalerite dominant textural style with an ore assemblage consisting of sp-gn-po-cte-qtz-chl±py±fe dol±cp. Sulphide has altered the shale host rock, mainly along foliations, or altered the infill assemblage between dilated bedding laminations. Where sphalerite alters the shale host rock it is accompanied by chlorite, which is most abundant in this setting, with minor quartz, pyrrhotite, calcite and ferroan dolomite. The infill assemblage, in approximate order of abundance, comprises galena, sphalerite, pyrite, calcite and quartz with accessory ferroan dolomite, chalcopyrite and pyrrhotite (Figs 15 c-f).

The other style of planar fracture breccias are foliation fill breccias, which occur within a single carbonaceous shale defined mesoscale competency domain (Fig. 14). Mineralisation occurs as fine veins along cleavages and consisting of cte-qz-sp-gn-py±fe dol±cp. Quartz and carbonate commonly have fibrous habits. Sphalerite frequently occurs along the margins of veins. It is also located in the interior of veins where it has replaced carbonates and then has locally been replaced by galena and euhedral pyrite (Figs 14 d and e). Cleavage hosted veins are commonly continuous with bedding parallel ones.

Fold clast breccias consist of clasts of folded and dismembered massive siltstone, mudstone and carbonaceous shale beds between unfolded massive siltstones and mudstones

(Fig. 16). Bedding included in the breccias is significantly thinner than in the enclosing rocks. In hand specimens, bedding is typically less than a centimetre thick but in underground exposures may be significantly greater than this and exceed several tens of centimetres in breccias that are several metres wide (Fig. 16). Several fold orientations and generations are present within the breccias but ones with east vergent and east-dipping axial planes, parallel to S_2 , are the largest and most abundant. The matrix consists of calcite, ferroan carbonate, quartz, sphalerite, galena, with minor pyrrhotite, pyrite and chalcopyrite (Figs 16 d-f). It occurs between layers in hinges, on the limbs of folds and in discontinuities that dismember layering. There is also significant alteration of the host rock clast in the breccias (Fig. 16e).

Foliation fill and fold clast breccias contain the same ore assemblage and are often located next to each other. They are typically a galena-rich textural style. Foliation fill breccias have a higher volume of clasts than the fold clast breccias. Quartz comprises between 10-30% of the fill and is slightly more abundant in the fold clast than the foliation fill breccias (Figs. 14). Crystals are anhedral to subhedral, between 20-350 μm , with the coarsest grains situated in areas where there has been the most dilation. They have straight to weakly undulose extinction and commonly a fibrous habit in fold hinges and bedding discordant veins. Quartz is most concentrated along the margins of infill areas. Boundaries with carbonates are simple but with sulphide aggregates are more complex due penetrating prismatic quartz terminations (Figs. 14 and 18).

Carbonate comprises up to 40% and 60% of fill in the foliation fill and fold clast breccias respectively. It is dominantly calcite with minor ferroan carbonate (Figs. 14 d and 16f). Grain shapes range from euhedral to subhedral with fibrous habits being common. Calcite is distributed evenly throughout the matrix and mutual grain boundaries with other carbonates and quartz are smooth. They are more irregular with sulphides.

Sphalerite and galena are the main sulphide phases in these breccias. Their abundance is variable with either being locally dominant. Sphalerite typically forms 15-30 % of the fill. Grains are subhedral to euhedral and between 70-300 μm (Figs 14 and 16). Sphalerite occurs as compact aggregates between layering. It contains inclusions of quartz and carbonate. It also occurs as fine aggregates and individual grains along carbonate and quartz grain boundaries and crystallographic cleavages, rounded inclusions in galena, or as concentrations around clasts and along wall rock contacts. Grain boundaries with other sulphides are simple but are complex with quartz and carbonate.

Galena forms 15-40% of the breccia fill as aggregates up to several millimetres with irregular shaped boundaries, and containing inclusions of quartz, carbonate, sphalerite and pyrrhotite (Fig. 18a). It has commonly replaced carbonates in host rock clasts and in matrix

infill where it is located along quartz and carbonate grain boundaries. Pyrite and pyrrhotite are minor sulphide phases in the breccia fill. Early microcrystalline pyrite is located in clasts (Figs 14d and 16f). Pyrrhotite grains are subhedral and typically larger than 100 μm . Euhedral pyrite is generally larger than 100 μm and is disseminated throughout galena-rich areas and contains inclusions of all other sulphide species (Fig. 18a). Chalcopyrite is an accessory phase that occurs as 50-100 μm subhedral to euhedral crystals in aggregates with galena and occasionally freibergite (Fig. 18b). Fine chalcopyrite occurs along sphalerite grain boundaries as grains less than 5 μm in diameter.

Rounded clast breccias typically contain less than 5 % rounded clasts of highly foliated carbonaceous shale up to several millimetres in diameter (Fig. 17). The matrix, which forms the bulk of the breccia, consists of ferroan dolomite, galena, quartz, sphalerite, pyrite and accessory feldspar. These breccias are typically 1-5 cm wide and situated between massive siltstone or mudstone wall rocks and fold clast breccias (Fig. 16c and 17a). Galena is located in 100-500 μm aggregates that may be elongated and contain remnant inclusions of sphalerite, quartz and ferroan dolomite. Quartz grains are 50-100 μm , anhedral, have undulose extinction and are distributed between ferroan dolomite grains. Ferroan dolomite is subhedral, between 100-500 μm and has eroded boundaries where it is in contact with sulphides. Sphalerite is subhedral to anhedral, between 10-70 μm and disseminated throughout the matrix along carbonate grain boundaries and as inclusions in galena. Pyrite is euhedral and coarse grained.

Copper breccias

The bulk of the copper orebody consists of foliation fill breccias but rare examples of the fold clast and rounded clast breccia styles can be found. Sulphides are arranged in a network of intersecting elongate aggregates along east- or west-dipping qz-dol veins located along shear bands (Fig. 19). The host rocks are composed almost entirely of 10-20 μm subhedral to anhedral quartz with minor 40-50 μm euhedral carbonate (Fig. 19). Chalcopyrite, pyrrhotite and pyrite as well as trace amounts of sphalerite and galena are located in east- or west-dipping quartz-dolomite veins along S_2 or S_3 cleavages (Fig. 19c). Quartz and dolomite commonly have a fibrous habit with fibres being vertically oriented.

Discordant veins

Steeply east-dipping carbonate, quartz and sulphide veins are a common feature transecting the barren host rock around the margins of Zn-Pb-Ag orebodies (Fig. 20). They have a similar orientation to, and the same shear sense as S_2 , where they are not surrounded by flanking structures and are commonly parallel to F_2 axial planes. Veins frequently terminate

against bedding parallel base metal bands. The veins formed by dilation of S_2 shear bands in D_4 and several vein opening episodes can be recognised in them (Part C). Fibrous and granular textured veins have the same mineralogy. Fibres are commonly sigmoidal with carbonate in the centre of the veins and quartz along the margins where there are also quartz selvages. The earliest mineral deposited in the veins was fine grained granular ferroan dolomite, which forms a matrix around angular wall rock fragments.

Transitional zones

The copper and Zn-Pb-Ag orebodies are separated by silica-dolomite alteration which envelopes the copper and is continuous with the Zn-Pb-Ag ores. Adjacent to the copper orebodies silica-dolomite alteration is discordant to bedding but becomes increasingly stratiform towards the Zn-Pb-Ag ores (Fig. 3c). The transitional area between the two contains coarse grained quartz, calcite and ferroan dolomite with sulphide replacing the carbonate. Microcrystalline pyrite is the oldest sulphide and is present as inclusions in sphalerite, pyrrhotite and chalcopyrite. The relative abundance of sulphides changes towards the Zn-Pb-Ag ores at the expense of chalcopyrite to favour sphalerite and galena. Sphalerite forms coarse rounded inclusions in galena, which is the same mutual relationship displayed in all the other textural styles. Chalcopyrite appears to overprint sphalerite, pyrite and pyrrhotite but all were deposited temporally close together (Fig. 21).

Distribution of the Ore Textures

The distribution of the various ore textural styles was determined from detailed logging of drill core from the southern side of the Zn-Pb-Ag orebody, close to the copper orebodies, through the orebody to the low grade areas in the north. The location of each band and, its thickness, composition and texture were recorded. The drill holes were projected onto a south-dipping plane normal to the long axis of the lens. The projection lines are parallel to the long axis of the lens to preserve the distribution of the holes relative to the metal distribution (Fig. 3). The cumulative thickness of sulphide bands, fine grained sphalerite microbreccias and galena-sphalerite breccias was plotted as separate graphs for each ore package (Fig. 22) and on maps that show their distribution and proportion in each ore package (Fig. 23). Microcrystalline sphalerite and fine grained sphalerite bands are combined because the latter form only a minor part of the deposit when considered separate from the fine grained sphalerite microbreccias and have similar distributions. Graphs of cumulative thickness similar to those in Figure 22 are plotted along the drill holes traces, which form the x-axis, in Figure 23. The ore packages are

continuous with conformable silica-dolomite alteration extending from bodies containing copper orebodies or with pyritic shales in the extremities of the deposit. North of the silica-dolomite alteration large areas of microcrystalline pyrite alteration have a subtle NW-SE-striking trend and are overprinted, at mine-scale, by the ore packages.

The graphs in Figure 22 show a north-westwards progression of the maximum cumulative thickness from east to west through the ore packages. The maps (Fig. 23) show this trend very clearly as a NNW-SSE-striking peak for the combined ore textural styles. Both the microbreccias and the other breccias have peaks that coincide with that of the combined ore textural styles. Conversely, the sphalerite bands have two NNW-SSE-striking peaks, one either side of the breccias and combined styles peak. With the exception of the microbreccias all styles have small NW-trending peaks adjacent to the silica-dolomite front. The percentage of each style in the ore package corresponds to the peak cumulative thickness but with the (non micro-) breccias having a broader distribution than the others.

The highest Pb+Zn grade parts of the ores correspond to the greatest cumulative thickness of breccias. Pb:Zn ratios decrease northwards away from the silica-dolomite front and the maximum of the combined cumulative thickness for all textural styles combined, which is consistent with the findings of Davis (2004). High grade intercepts through lens K have a NNW-SSE trend, which is matched by the maximum cumulative thickness of ore bands and of individual textural styles (Figs 22 and 23). Microcrystalline pyrite and ferroan dolomite alteration are also located throughout the lens.

Microstructures

In all textural styles the ore assemblage is located in either alteration zones along tectonic cleavages or infill veins along cleavages or bedding planes. Table 1 lists each ore textural style and the structural settings of the ore and their associated alteration minerals.

Nodular layers

Porphyroblasts that make up these layers are located along strike from the low strain areas between crenulation cleavages in the adjacent layers. The nodular layers are not deformed by the cleavages, which cannot be traced across them (Fig. 13).

Microcrystalline pyrite

The anastomosing pattern in the microcrystalline pyrite bands is produced by pyrite located along crenulation and crenulated cleavages in shaly layers. Consequently, the pyritic

shales are extremely useful in studying the deformation history as they partially preserve crenulation patterns in which several generations of cleavages can be recognised. Linear seams correspond to the differentiated or limb domains of the cleavages and curvilinear ones to hinge regions. Pyrite is texturally identical in the limb and hinge areas and appears to have been deposited after formation of the S_4 cleavage. This timing is corroborated by structural and paragenetic relationships in east-dipping carbonate veins that formed in D_4 and involved several episodes of brecciation (Part C). The presence of microcrystalline pyrite in the younger breccias clasts, but not the older ones, indicates this alteration took place between the two brecciation episodes as the clasts appear to have been derived from the same layer nearby (Part C).

Microcrystalline sphalerite

Microcrystalline sphalerite displays two important microstructural features. The first is the alignment of aggregates along S_2 , S_3 , and rarely S_4 (Fig. 5). The relative abundance of the different generation of cleavages represented in the network of sphalerite aggregates may reflect the density of each cleavage and/or their orientations relative the maximum principal stress at the time of mineralisation. Microcrystalline sphalerite in the near massive bands overprints disjunctive cleavages that displace the massive mudstone host rock without any apparent deformation of the sulphides. Other microstructural feature are alteration fronts of microcrystalline sphalerite extending out from discordant qz-cb-sp-po-gn±cp±py veins hosted by disjunctive S_2 (Fig. 24).

Fine grained sphalerite

There is a range in the amount of disruption of bedding in fine grained sphalerite bands ranging from sphalerite filled crenulation cleavages in laminated shales to microbreccias, which are microscopic versions of the galena-sphalerite breccias in terms of the pattern of brecciation (Figs. 8). Elongate aggregates in the fine grained sphalerite bands overprint tectonic cleavages, most notably S_4 (Fig. 8b). Alteration fronts in these bands coincide with the boundaries of deformation domains. Figure 8a shows a sphalerite alteration front that coincides with a fold in bedding. Attenuation of adjacent layering shows the sphalerite is located in the area where deformation was greatest. Microbreccias contain host rock clasts and ankerite veins that predate sulphide mineralisation. The two sphalerite grain size domains in the fine grained sphalerite bands and microbreccias reflect variations in structural setting (Fig. 9). The finer distribution corresponds to alteration of host rock clasts and the other to infill where there has been dilation.

Galena bands

The anastomosing patterns in galena bands are similar to that in the pyritic shales and by analogy are inferred to form by overprinting cleavages in some layers. The presence of anastomosing pyrite seams show that galena is overprinting a deformed rock.

Foliation fill breccias

The foliation fill breccias form by infill along S_2 and S_3 cleavages within a single competency domain or rock type (Figs 14 b and c). A ubiquitous characteristic of veins in these breccias is the different orientation of layering on either side. This indicates that dilation occurred at the boundary of two differing strain domains. The dilation process is discussed later.

Fold clast breccias

The bulk of mineralisation in the fold clast breccias consists of infill between layering around disharmonic folds. There is minor infill along foliations and replacement along foliations in the clasts. Folding is contained within interbedded laminated shales and finely interbedded bedded shales, siltstones and mudstones between unfolded siltstones and mudstones with significantly thicker bedding. Within the breccias, folds are also localised along strike from disjunctive cleavages in the adjacent massive siltstones and mudstones, with the intensity of folding decreasing away from these structures along the layering. Folding may be isolated in pockets or continuous along the layers depending on the spacing of disjunctive cleavage in the enclosing units (Fig. 25). The axial planes of the folds are east verging and commonly folded. They have near vertical and east-dipping segments with the latter orientation being the dominant one.

Within the fold clast breccias the bulk of the ore assemblage was deposited between layering around disharmonic folds (Fig. 25). The axial planes of the dominant folds within the breccias are generally folded and vertical to east-dipping. Smaller scale folds may have different orientations to the dominant folds. Gently and tightly folded layers have different cleavage relationships. Tight folds have axial planar foliations that display the opposite shear sense on either limb, but microstructural examination shows they are not the same generation. The foliation west of an anticline is S_2 , and is east-dipping with east block up (or, top to the west when shallow-dipping) shear sense. S_2 is folded around the hinge and into the axial planar foliation on the other limb, which is S_3 . On both limbs the axial planar cleavages are overprinted by vertical S_4 (Figs 25-27). In gently folded layers, S_2 is parallel to the axial plane on long limbs, but on short limbs there is no axial planar foliation, S_3 is west-dipping and S_2 is rare. S_4 is

vertical on both limbs. There is a paucity of S_3 on the long limbs in both the gently and tightly folded layers.

Rounded clast breccias

Few useful microstructures are preserved within the rounded clast breccias, apart from strongly foliated host rock clasts. The setting of these breccias at a larger scale suggests that they are related to the fold clast breccias, because they are commonly located between these and the unfolded wall rocks, or occur as patches within either these or foliation fill breccias (Fig. 16c).

Asymmetric boudin breccias

The formation of the asymmetric boudin breccias is covered in detail in Part C. The microstructures pertaining to mineralisation are the same as for the fine grained sphalerite bands. The infill lies between unfolded to very gently folded layers. Both walls of the bedding parallel veins are crenulated but never to the same degree. One side will commonly be crenulated by S_4 and the other by an older cleavage.

Discussion

The NNW-SSE-trending orientation of the textural distribution is parallel to

1. the mine-scale orientation of the copper orebodies
2. the enveloping silica-dolomite alteration bodies to the copper orebodies
3. D_4 fold hinges and
4. the large scale Zn-Pb-Ag metal distribution (Part A).

These relationships are indicative of a structural control on the development of the Zn-Pb-Ag orebodies. The Zn-Pb-Ag orebody is texturally zoned from a core of breccia outwards to banded textural styles. Accompanying this zonation is a change in the dominant depositional style from infill to alteration. This zonation represents a change in the scale of structure hosting the ore minerals. Outwards from the core the host structures are smaller, changing from layering to foliations. Such a change will be accompanied by a variation in the fluid-rock ratio to lower values and this is reflected by a decrease in the abundance of galena relative to sphalerite. This illustrates the interaction between the structural geology and geochemistry of the mineralising system. The commonality of the orientations of all textural styles is further evidence against the occurrence of remobilisation.

Base metal mineralisation is recognised as comprising four stages. Initial deposition of ankerite in the discordant and mostly east-dipping veins was followed by widespread deposition of microcrystalline pyrite along foliations. The third stage involved deposition of calcite and quartz, mainly in veins, but also involving alteration of earlier carbonates. Base metal sulphides were deposited in the fourth stage. The overprinting sequence in this last stage started with the deposition of sphalerite, pyrrhotite and chlorite, followed by galena, chalcopyrite and freibergite, and concluded with pyrite and quartz as the final minerals to be deposited. Significant parts of the sequence are recognisable in all ore textural styles, demonstrating their close timing relationship. The occurrence of initial base metal sulphide deposition during the last stage of the sequence, and the presence of only a single phase of deposition for galena and sphalerite, shows there has been no redistribution of metals since mineralisation.

Sulphide mineralisation is constrained by overprinting structural relationships to the fourth regional deformation. The earliest sulphides were deposited during the formation of the discordant ankerite veins. Dilation of these veins was related to shearing strain along S_4 as discussed in Part C. Microcrystalline pyrite is the oldest sulphide in the deposit, and is widely interpreted to be related to base metal mineralisation (Blanchard and Hall, 1937; Love and Zimmerman, 1961; Perkins, 1998; Painter et al., 1999; Chapman, 2004). Love and Zimmerman (1961), Painter et al. (1999) and Chapman (2004) placed a pre-deformation timing on microcrystalline pyrite mineralisation, but cleavage overprinting relationships show that this is not correct. Painter et al. (1999) interpreted wavy seams of microcrystalline pyrite to show mineralisation occurred before deformation, but the overprinting relationship of this sulphide to tectonic cleavages shows this was not the case. The feature described by these workers is the result of pyrite deposition along deformed foliations. Similarly, Love and Zimmerman (1961), Solomon (1965) and Neudert (1986) attributed framboidal microcrystalline pyrite habits to biological activity, placing a diagenetic timing on mineralisation. However, the tectonic timing precludes such an interpretation of the microcrystalline pyrite habit, which is better explained by chemical conditions around the time of mineralisation. Experimental work by Butler and Rickard (2000) showed that framboidal textures form in the absence of biological activity by rapid nucleation in hydrothermal environments where pyrite is strongly supersaturated. Where pyrite supersaturation is low, single crystals form. Although these workers investigated the formation of frambooids in the diagenetic environment, their work shows that the formation of either a framboidal or euhedral crystal habit is linked to the saturation of components during and after nucleation, rather than biological activity. Under such conditions the association of quartz with euhedral pyrite is indicative of low pyrite supersaturation, possibly by dilution caused by a

higher fluid flux. Framboidal textured pyrite and a paucity of other associated alteration minerals reflects restricted flow conditions and continuing high pyrite supersaturation.

The textural relationships of the microcrystalline pyrite show it was deposited slightly before base metal sulphide mineralisation but was paragenetically separated from it by calcite-quartz deposition. At the scale shown in Figures 3b and 23, the base metal sulphide distribution overprints the microcrystalline pyrite bodies and demonstrates a relationship that is consistent with that at the microscopic-scale. The timing of microcrystalline pyrite deposition restricts the maximum age of base metal mineralisation to early D₄ onwards. The microstructural relationships in the ore textures shown here, and the high representivity of this study, demonstrate mineralisation occurred in D₄ and there was no micro- to macroscale remobilisation. This is consistent with deposit-scale studies examining metal distribution and orebody geometries presented in Part A. According to Chapman (2004) there is very little textural variation between Mount Isa and the Hilton and George Fisher deposits located some 20 km north. It is therefore likely that all deposits have the same timing, as was initially proposed by Perkins and Bell (1998).

Copper and Zn-Pb-Ag mineralisation were synchronous. Both orebodies contain similar sulphide-structural overprinting textures with directly comparable microstructural relationships. However, individual textural elements in the copper ores are larger than their Zn-Pb-Ag equivalents (e.g., foliation fill veins). The continuity between the Zn-Pb-Ag ore packages and stratiform silica-dolomite protrusions that extend from the main discordant bodies is further indication of a relationship between the copper and Zn-Pb-Ag orebodies. The change from discordant to stratiform silica-dolomite alteration demonstrates a change from discordant to concordant structures controlling deposition at the mine-scale. Perkins (1997) also proposed a link between the copper and Zn-Pb-Ag mineralisation and suggested that the different orebodies are the result of zoned deposition from the same hydrothermal system. It was not possible in the present study to determine the nature of the mineralising fluid(s), but the interpretation that all the base metal arrived at the depositional environment in the same hydrothermal fluid is the most straight forward explanation for all the currently known features of the deposit. The findings of the present study, including the possibility of all base metals being transported in the same fluid, are in accordance with fluid studies by Waring (1990), where it was demonstrated that mineralising fluids moved from the south to the north of the deposit.

Perkins (1984) and Swager (1985) defined the paragenetic sequence for the copper ores. They found metasomatism commenced with dolomite recrystallisation and widespread silicification followed by dolomitisation and then copper mineralisation, which involved the deposition of chalcopyrite, Fe sulphides, quartz and chlorite. Fluid flow directions for copper

mineralisation were upwards from the Basement Fault and to the north (Perkins, 1984; Bell et al., 1988; Waring, 1990). Synchronous copper and Zn-Pb-Ag mineralisation means that the copper alteration system will impact on the Zn-Pb-Ag one. Material movement during copper mineralisation and associated metasomatism involved silica introduction and dolomite loss during dolomite recrystallisation and silicification, and sulphur, copper and possibly iron addition in the last stage. In the Zn-Pb-Ag orebody, the first phase of alteration introduced ankerite, the second sulphur and iron the third calcite and quartz and the final, zinc, lead, copper, iron, silver, sulphur and quartz. Ankerite in the first stage of Zn-Pb-Ag mineralisation may have been derived as exhaust products from silicification due to the first stage of alteration during copper mineralisation. Iron in the microcrystalline pyrite may also be the result of alteration of the host rocks in the copper orebody. The change from iron being deposited in carbonates to sulphides may indicate the introduction of a sulphur source separate to the one bringing the quartz and Fe-carbonate components. This plus the sulphur isotope signatures recognised by Painter et al. (1999), which indicate a common sulphur source for all the sulphides in the deposit, may indicate a fluid mixing process whereby one fluid introduced sulphur and another the metals. The deposition of calcite may indicate the depletion of iron by the deposition of microcrystalline pyrite.

Examination of the ore textural styles shows that all sulphide deposition was structurally controlled. Fluid pathways include along tectonic foliations and bedding with permeability of the structures enhanced by increasing their apertures during ductile deformation that involved cleavage formation and reactivation of older foliations. Mineralisation occurred by either alteration centred on foliations or infill along bedding or tectonic cleavages to form simple planar or complex curvilinear vein geometries.

Sulphides that were deposited along foliations where there is little evidence for infill are interpreted to indicate an alteration mineralisation style. This style of mineralisation is present in nearly all the ore textural styles in the deposit but forms the bulk of the microcrystalline sphalerite, microcrystalline pyrite and rounded clast breccias styles. It is also a significant component of the asymmetric boudin breccias and the fine grained sphalerite bands. There are no obvious features associated with this alteration style of mineralisation that precisely indicate the kinematic processes that contributed to the permeability of the host structures beyond their misorientation with respect to the maximum principal stress at the time of mineralisation (cf. Cox et al. 2001).

Veins formed where adjacent rock volumes were deforming differently. Progressive shearing strains cause rotations of the deforming bodies in which they are located and can be accommodated by either actively forming or reactivating foliations (Bell, 1981). The difference

in the deformation of adjacent blocks causes the rotation of one relative to the other and is shown by foliations of the same generation having slightly different orientations either side of the veins. Variations in progressive shearing strain that led to differential block rotation can be caused by changes in the density or orientation of active foliations. This generally results from shearing along different generations of foliations in either layer during the same event. The differential rotation of adjacent volumes can cause space problems between adjacent domains. These can be resolved by dilation along their mutual boundary, where new material fills the void, or by repartitioning the deformation. Consequently, evidence of such unstable deformation is only preserved if dilation can occur, which depends on the addition of material needed to fill the increased volume. Dilation occurs along a suitable oriented pre-existing structure where they are present. Alternatively, new structures form, most likely by cataclastic flow. The simplest examples of this process are the formation of planar veins (Fig. 28). In some cases it is possible to identify the structures that actively caused dilation, such as shearing along a specific cleavage on one side of the vein as is the case with the nodular layers and bedding parallel veins. In these cases progressive shearing strain along S_4 caused dilation. Microporphyroblasts of quartz, carbonate and sulphides in the carbonaceous shales are located between layers where different foliations accommodated the progressive shearing strain component of the deformation. Generally in one layer there will be reactivation of a cleavage other than the one which is active in the adjacent layer (e.g. Fig. 26).

Dilation was also a means of resolving space problems between areas of differential strain in the fold clast breccias; however, the link to fold development complicates the process. Dilation occurred during the last stage of folding. Folds in the breccias are composite structures formed by overprinting inhomogeneous strain during a series of deformations. The formation of these folds is determined from overprinting cleavage relationships and is similar to that described in Part B for mine-scale folds that control ore shoots within the deposit. The process of folding commenced in D_2 with the formation of vertical S_2 with an east block up shear sense, causing westwards rotation of bedding (Fig. 29). D_2 strain was inhomogeneously distributed between the different rock types and formed a disjunctive cleavage in the massive siltstones and mudstones enclosing the breccias. S_2 is a distributed crenulation cleavage in the interbedded shale and siltstone units within the breccias that is localised along strike from its equivalent disjunctive cleavage in the adjacent layers. This effectively localises the fold clast breccias around disjunctive S_2 , and is especially apparent where the breccias only persist along layering for short distances. D_3 structures were localised, with strain variations between and along layering. It formed discordant horizontal shear bands that are restricted to competency domains defined by rock type. Layering and S_2 in the shear bands were rotated into shallowly west-

dipping to horizontal orientations by top to the east shear sense along S_3 (Fig. 29a). Outside of the D_3 high strain zones reactivation of bedding rotated S_2 into east-dipping orientations while remaining largely unchanged itself (Fig. 29a).

D_4 formed a vertical NNW-SSE-striking cleavage, S_4 , that caused much of dilation in the fold clast breccias. The shear sense on S_4 was determined by the orientation of bedding, which was the result of preceding deformation including reactivation of some foliations early in D_4 , most notably east-dipping S_2 . The upper angle of rotation between S_4 and S_0 on the long limb of the fold in Figure 25 indicates that the latter was east-dipping prior to the formation of the D_4 cleavage. Bedding could only have been rotated into this orientation by reactivation of the east-dipping S_2 early in D_4 . Where S_0 is west-dipping, on the long limbs west of anticlinal hinges, S_4 has an east block up shear sense. On short limbs and long limbs where there has been reactivation of S_2 , and where S_0 is horizontal or east-dipping, S_4 has an east block down displacement. Inhomogeneous reactivation of S_2 on the long limbs formed bedding parallel veins between layers and qz-cb-sulphide microporphyroblasts within them (Fig. 25).

Inhomogeneous strain between layers with different competencies formed disharmonic folds that were centres of dilation and mineralisation in the last stage of their development. Folds were initially formed by rotation of bedding in D_3 shear bands. These were tightened in some layers during later deformation. Disharmonic folds formed where strain in the D_3 shear bands was more concentrated in one bed compared with those adjacent. This resulted in a narrower shear band with a higher angle of rotation of earlier foliations in layer that experienced more intense deformation. S_4 formed with an east block down shear sense in the vicinity of the S_3 high strain zone in the layer that was more intensely deformed during D_3 . This rotated it clockwise (looking north) and tightened the initial D_3 fold. In the adjacent layer, where S_3 is not as intense and bedding was still moderately west-dipping, S_4 formed with an east block down shear sense and may not have been intense so the finite fold has a higher interlimb angle. The opposite shear sense on S_4 rotated the layers apart to produce the curvilinear veins.

The kinematics involved in forming the rounded clast breccias are difficult to determine because only a small amount of the host rock is preserved in the breccias. The roundness and fine grained nature of the clasts could be formed by milling-type processes but patches of rounded clast breccia among other breccia styles suggest this is unlikely. A more likely explanation is that the rounded clast breccias are examples of extreme alteration that has overprinted high strain zones. Breccias are situated in units that have a lower competency than the surrounding rocks and the rounded clast breccias are commonly located along the margins of these adjacent to the enclosing massive siltstone or mudstone wall rocks. This indicates that they are located in high strain areas because shearing strain tends to be localised along the

margins of competency domains because of mechanical instabilities caused by one domain having a higher strain rate than the other (Goodwin and Tikoff, 2002). Dilation has been shown to result from increasing the aperture of pre-existing structural heterogeneities. In the case of the rounded clast breccias, the high strain fabric facilitated extremely high permeability resulting in nearly complete alteration of the host rocks. Additionally, the mosaic textured matrix shows no sign of grain size reduction by cataclastic deformation.

Inhomogeneous deformation was extremely important in the formation of the Mount Isa deposit. Partitioning of deformation between competency domains defined by rock type produced the mesoscale stratiform sulphide textures that have been widely misinterpreted to be diagnostic of pre-deformation mineralisation (e.g. Love and Zimmerman, 1961; Valenta, 1994; Neudert, 1986; Painter, et al., 1999; Large et al., 2002; Chapman, 2004). Sequentially overprinted inhomogeneous deformation was responsible for the formation of complex structural heterogeneities, such as the folds that were major centres of dilation at all scales. The structural mechanisms controlling mineralisation at Mount Isa have implications for other structurally controlled deposit styles located in settings where there is a component of ductile deformation.

Conclusions

All sulphide textures in the Mount Isa Zn-Pb-Ag orebody are structurally controlled. Their formation can be linked to the deformation history by microstructural kinematic analysis that shows mineralisation occurred in D₄. The same kinematic processes of dilation also occurred in the copper orebody demonstrating that copper and Zn-Pb-Ag mineralisation occurred in the same deformation. Sulphides were deposited by replacement of carbonates or earlier sulphides either along tectonic foliations or in veins. In the case of deposition along foliations, permeability was primarily the result of their misorientation with respect to the maximum principal stress, but may have also been effected by ductile deformation surrounding the host structures. Veins developed to accommodate inhomogeneous strain in adjacent volumes either side of the host structure. The different deformation between the blocks involved inhomogeneous formation or reactivation of foliations and causes them, in the presence of a fluid, to rotate apart to form a vein.

Deformation was spatially partitioned between and within layering, which defined the dominant competency domains. Sequentially overprinting inhomogeneous deformation created structural heterogeneities that eventually formed disharmonic folds and dilation throughout the rock. Mesoscale bedding parallel sulphide textures reflect the control of rock type on strain

localisation that led to dilation and is not diagnostic of pre-deformation mineralisation as has been suggested. Consequently, this raises doubts about genetic models and data interpretation for other deposits that are based on such textures representing pre-deformation mineralisation.

Acknowledgements

The author gratefully acknowledges his supervisor Prof. Tim Bell. This project was funded by MIM Limited and initiated by Alice Clarke and Steve Law. Company geologists are thanked for their assistance in the field.

10. Tables

Table 1: Characterisation of Depositional Site and Style of the Ore Assemblage in the Ore Textural Styles.

Textural Style	Structural Setting
Nodular layers	Infill veins along bedding planes
Microcrystalline pyrite	Alteration along foliations
Microcrystalline sphalerite	Alteration along foliations
Fine grained sphalerite: Bands	Alteration along foliations Infill along foliations
Microbreccias	Infill veins along foliations Alteration along foliations Infill veins along bedding planes
Galena bands	Alteration along foliations
Discordant veins	Infill veins along foliations
Foliation fill breccias	Infill veins along foliations <i>minor</i> : Infill veins along bedding planes Alteration along foliations in clasts
Fold clast breccias	Infill veins along bedding planes <i>minor</i> : Infill along foliations Replacement along foliations in clasts
Rounded clast breccias	Infill along bedding planes <i>and likely</i> , Infill along foliations <i>minor</i> : Replacement along foliations in clasts

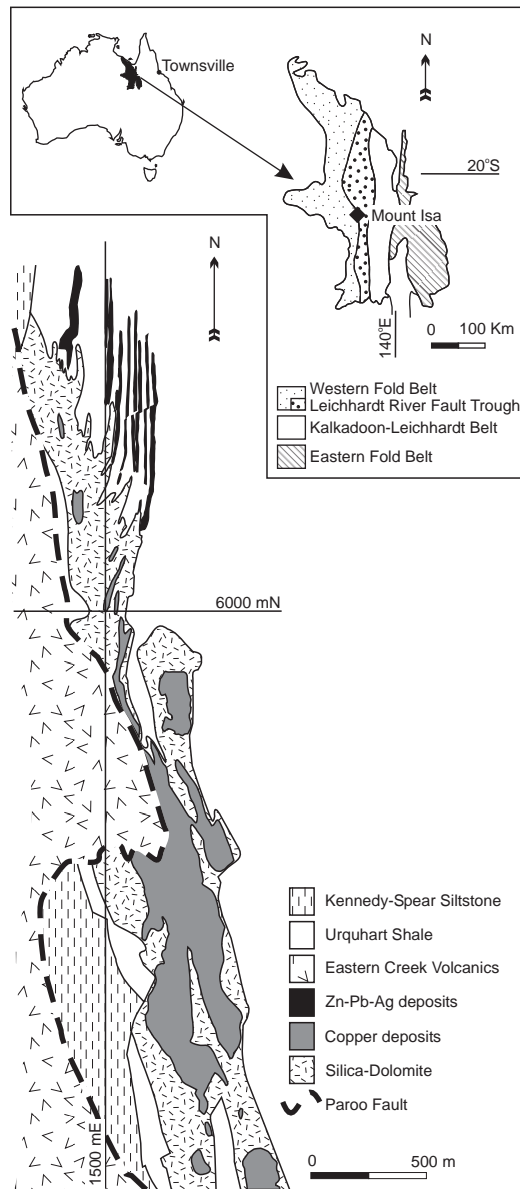


Figure 1: Plan of the Mount Isa Cu-Zn-Pb-Ag deposit at level 17 (2610 mRL) showing the distribution of the copper and Zn-Pb-Ag orebodies. Copper ores are contained within a quartz-dolomite alteration envelope. The Zn-Pb-Ag orebody contains ten ore lenses and is located north of the discordant body of quartz-dolomite alteration. Inset of the Mount Isa Inlier and its main tectonic units.

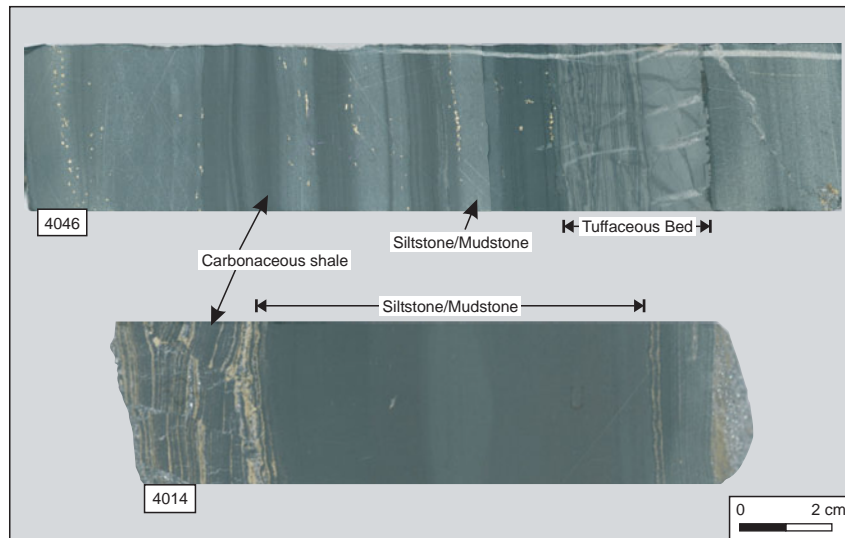
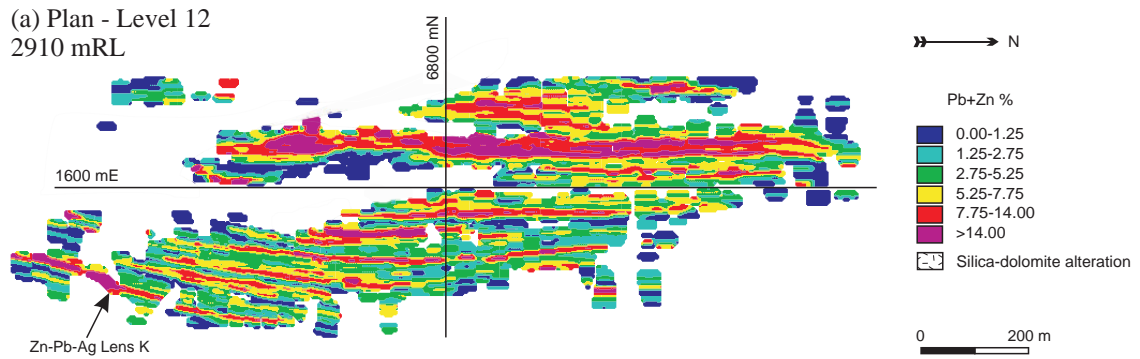
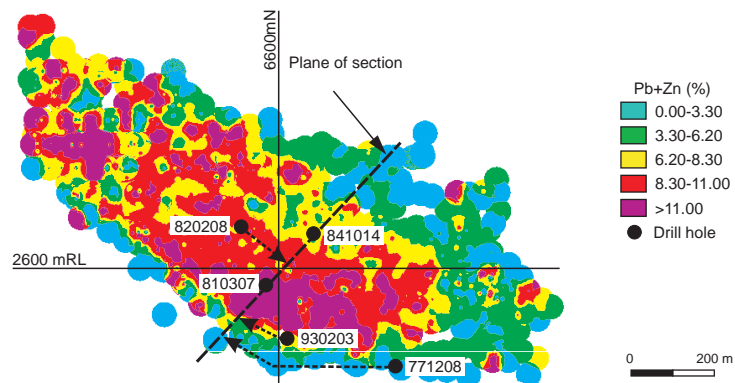


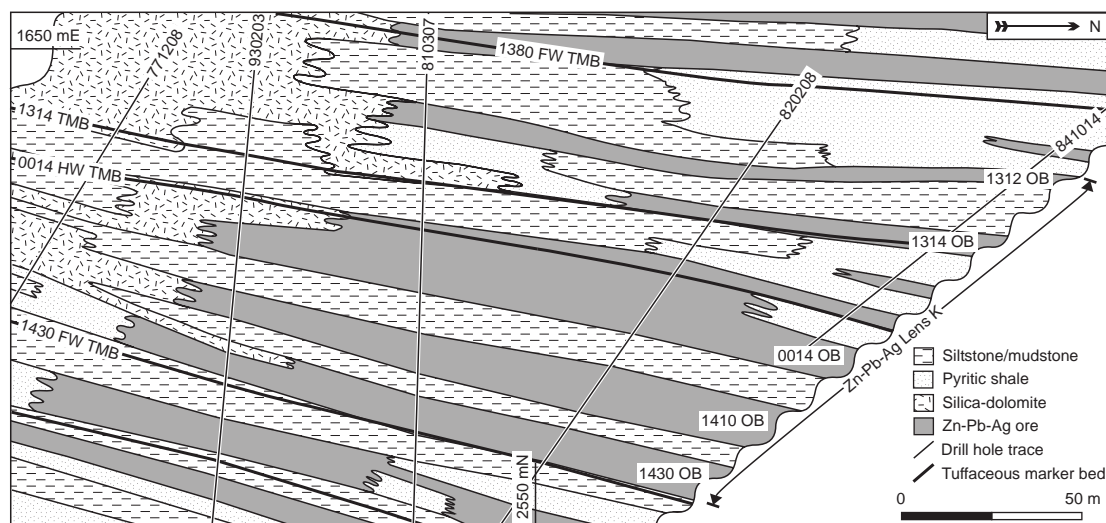
Figure 2: Interbedded sedimentary host rock types, carbonaceous shale, siltstone, mudstone and tuffaceous beds. The upper sample contains thinly bedded massive siltstones and mudstones interbedded with carbonaceous shales, and the lower one has a thick-bedded massive siltstone right of a brecciated carbonaceous shale. Dill core is 35 mm wide.



(b) Longitudinal Section - Lens K
Looking West



(c) South-dipping section



(d) Drill core

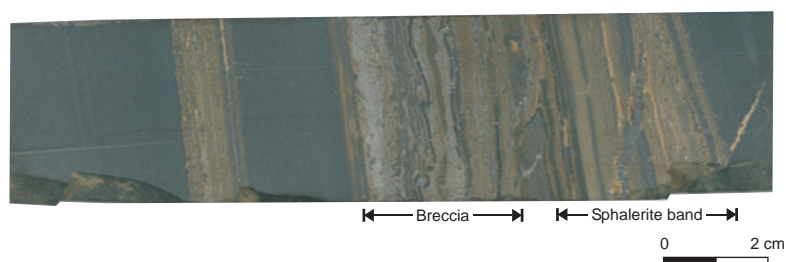


Figure 3: a) Plan of modelled Pb+Zn grade distribution on level 12 (2908 mRL) demonstrating the deposit contains ten lenses arranged in a NNW-SSE-striking en echelon array. Lens K is located on the eastern side of the deposit. b) Longitudinal section looking west of lens K, showing the location of the drill holes examined and how they are projection onto a south-dipping section normal to the long axis of the lens. The dashed arrows show the projection paths of the holes. c) South-dipping section of lens K. It shows that the lens contains five ore packages with their designated names as defined for mining operations. The Zn-Pb-Ag ore packages are continuous with stratabound silica-dolomite alteration bodies that extend from the large bodies of the same alteration hosting the copper ores. In places the Zn-Pb-Ag lenses are also continuous with the pyritic shales. d) Photograph of an individual sulphide band. The ore packages are collections of these bands.

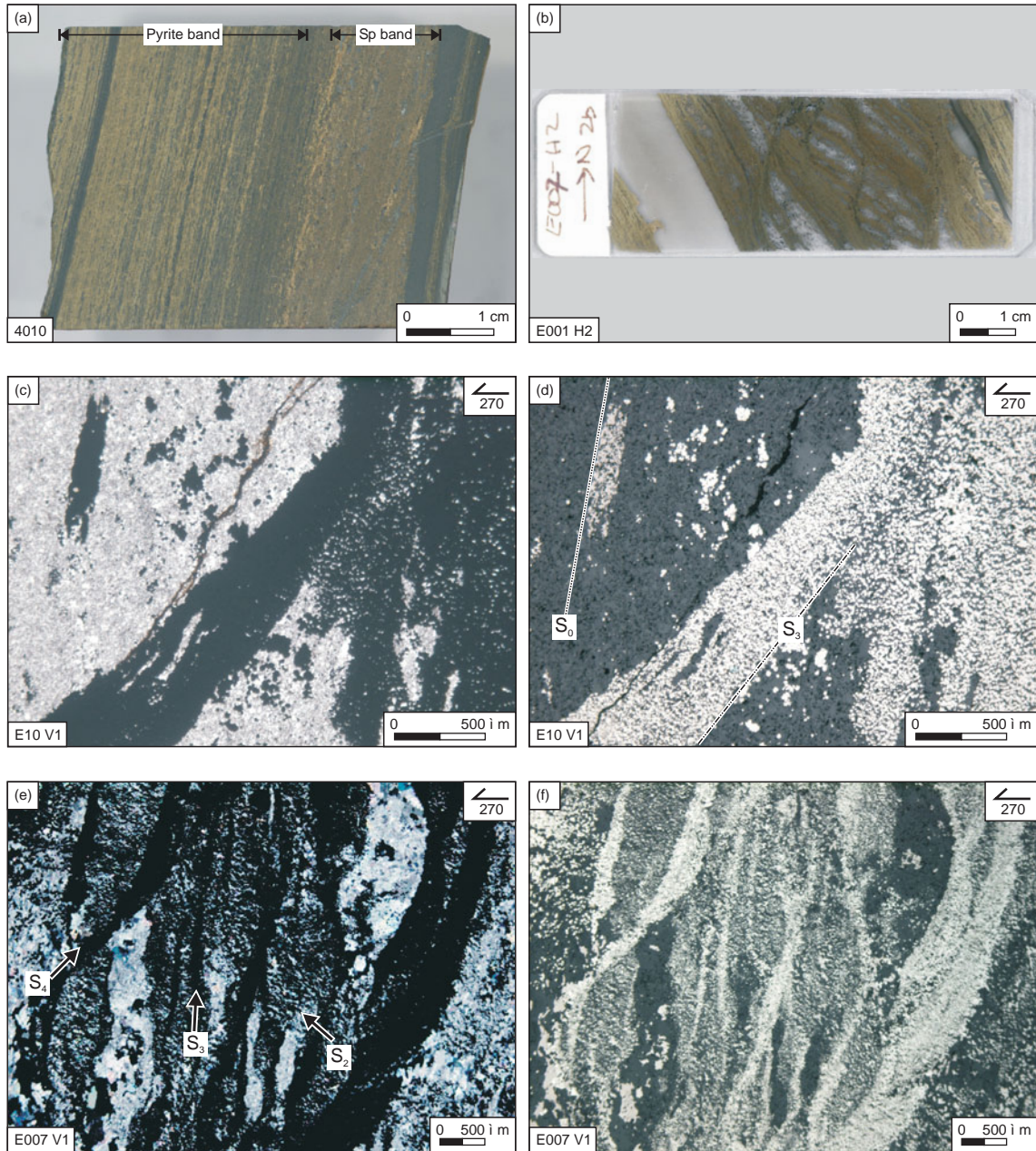


Figure 4: a) Microcrystalline pyrite band (left) and fine grained sphalerite band (right). Drill core is 35 mm wide. The laminated fabric of pyrite band is most obvious where pyrite is least abundant. b) Thinsection of a microcrystalline pyrite band where the anastomosing seams are coarse enough to make them out unaided by magnification. c) Microcrystalline pyrite in a west-dipping disjunctive cleavage, probably S_3 . Bedding is steeply west-dipping. Vertical section, transmitted light photomicrograph. d) Within the seams microcrystalline pyrite grains are aligned in horizontal and east-dipping folia. Reflected light photomicrograph of the area in (c). e) Microcrystalline pyrite overprinting S_4 and a crenulated foliation with quartz and carbonate between pyrite seams in Q-domains. Vertical section, transmitted light photomicrograph. f) Reflected light photomicrograph of (e).

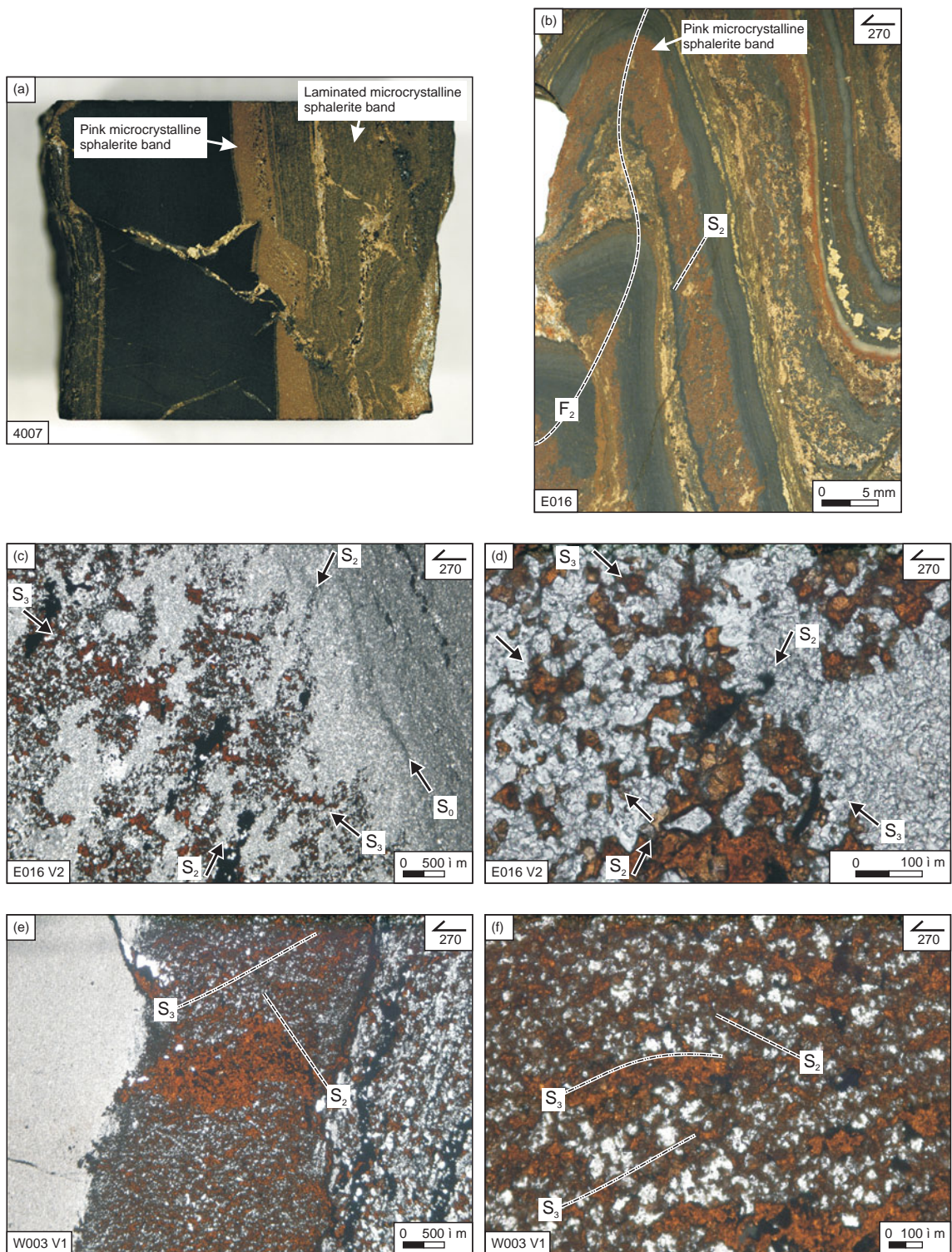


Figure 5: Microcrystalline sphalerite. a) Pink band of near massive microcrystalline sphalerite (centre and left) and a laminated band of microcrystalline sphalerite to the right. Drill core is 35 mm wide. b) Faintly visible west-dipping elongate aggregates of microcrystalline sphalerite in the pink bands. c) Photomicrograph of the sphalerite band in (b). The host comprises massive ferroan dolomite mudstone. Sphalerite and pyrrhotite in mainly west-dipping and lesser east-dipping compact elongate aggregates. d) Higher magnification of sphalerite aggregates in (b) and (c) shows carbonate in the vicinity of the sulphides is coarser than that distal to them. e) Photomicrograph of pink microcrystalline sphalerite band with laminated microcrystalline sphalerite (right). The patch of near massive sulphide (centre) contains inclusions of pyrrhotite. f) East- and west-dipping elongate compact sphalerite aggregates at high magnification. Vertical section, transmitted light photomicrograph (ppl).

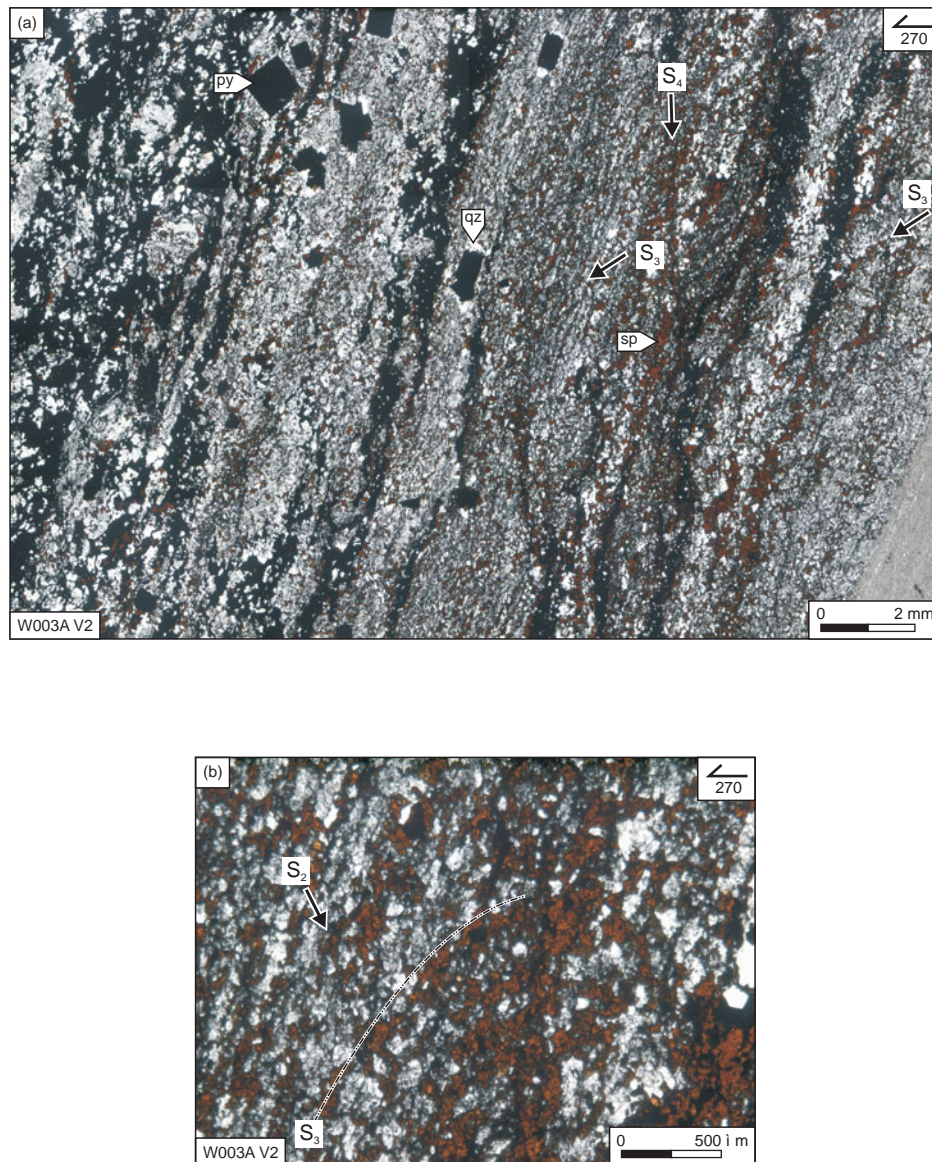
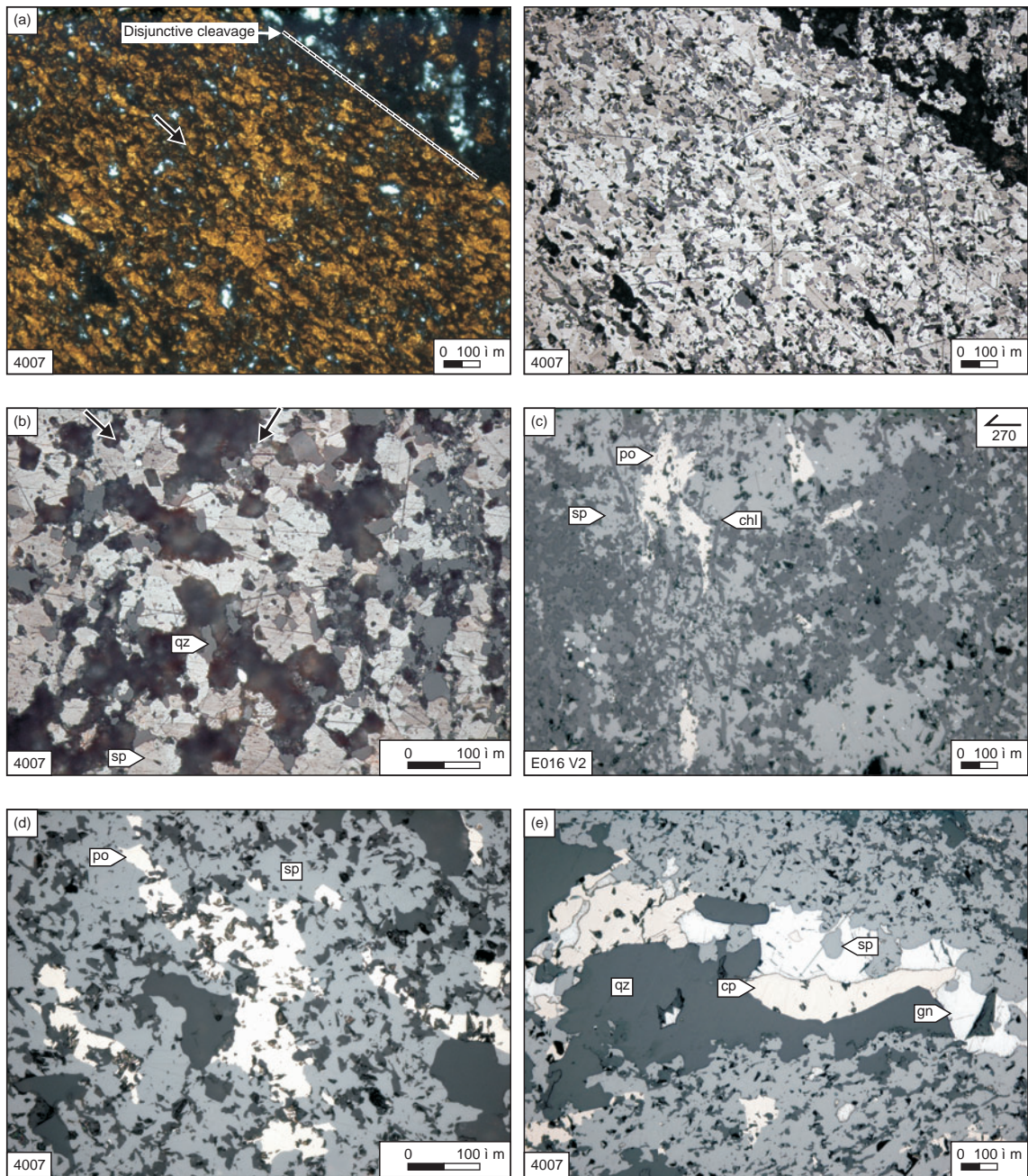


Figure 6: Laminated microcrystalline sphalerite bands. a) Collage of carbonaceous shale with microcrystalline sphalerite in elongate aggregates and coarse euhedral pyrite with quartz beards. Vertical section, Transmitted light photomicrograph (ppl). b). Elongate aggregates of sphalerite that comprise the laminated microcrystalline sphalerite bands with carbonaceous shale host rock (see also figure 5). Vertical section, Transmitted light photomicrograph (ppl).



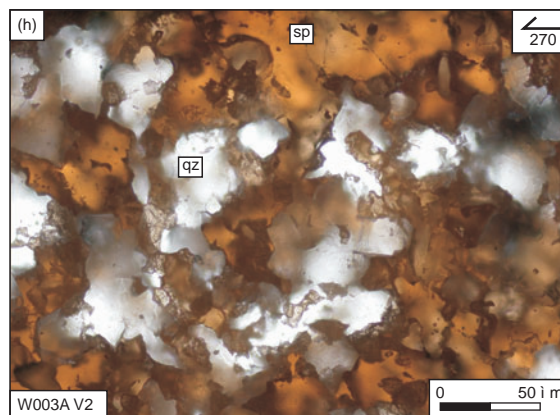
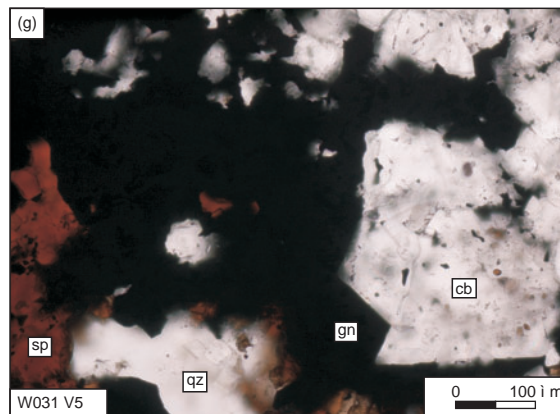
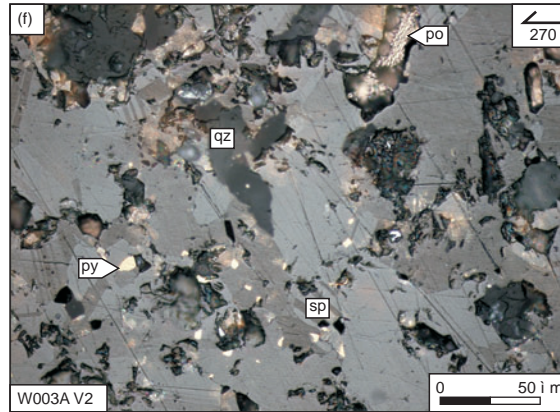


Figure 7: Microcrystalline sphalerite petrography. a) Etched near massive sphalerite in pink band (transmitted light left, and reflected light right) demonstrates the elongated nature of the aggregates, which is parallel to a disjunctive cleavage (probably S_2). Grain boundaries and twinning revealed by etching in the reflected light image shows a lack of shape or lattice preferred orientation sphalerite. b) Etched laminated microcrystalline sphalerite band. Sphalerite is situated in elongate compact aggregates with a lack of shape or lattice preferred orientation. c) Sphalerite and pyrrhotite intergrown with chlorite. Reflected light photomicrograph. d) Elongate pyrrhotite aggregates in near massive microcrystalline sphalerite. e) Sulphide overprinting relationships in the microcrystalline sphalerite bands. Sphalerite inclusions in galena indicate it is the older of the two. Galena and chalcopyrite display mutual embayments, which indicates they were deposited at nearly the same time. The location of chalcopyrite between galena and quartz indicates it exploited this grain boundary and a slightly later timing is inferred from this. f) Pyrite along sphalerite-sphalerite grain boundaries (etched sample, reflected light photomicrograph).g) Straight mutual grain boundaries of non-sulphides with sulphides. h) Complex mutual grain boundaries between quartz and sphalerite.

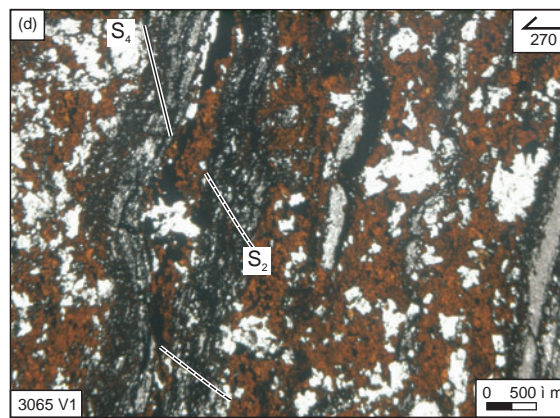
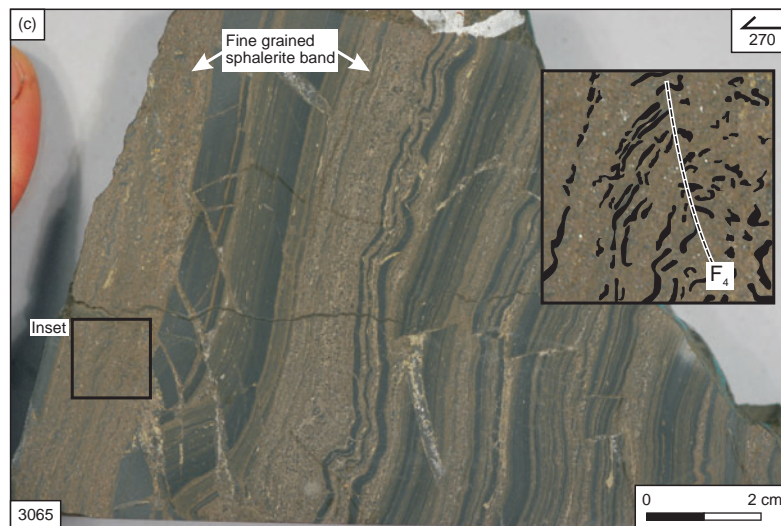
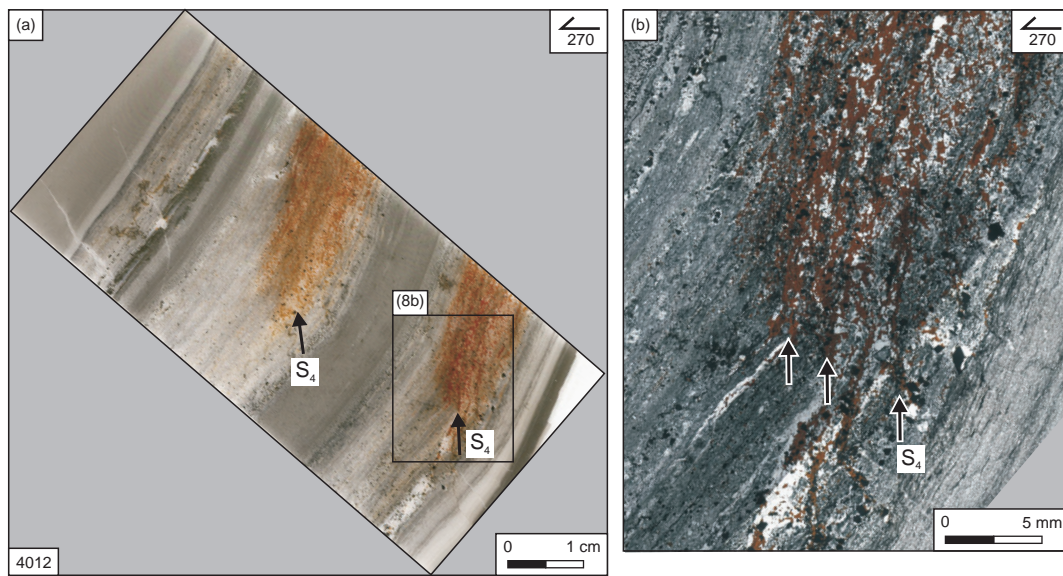


Figure 8: Fine grained sphalerite bands. a) Fine grained sphalerite band with minimal disruption of layering. Sphalerite alteration stops where there is a fold in the siltstone layer between the two sulphide bands. Vertical section, photograph of thinsection. b) Sphalerite and accompanying calcite and quartz alteration are situated in elongate aggregates that overprint S_2 and S_4 . Vertical section, transmitted light photomicrograph collage. c) Fine grained sphalerite microbreccia. In the inset the host rock clasts have been traced in black and define folded layering which shows there has not been significantly transported. d) Photomicrograph of fine grained sphalerite microbreccia. Shale and siltstone clasts contain tectonic cleavages and are folded. The layers on the left show dilation between them is related to folding.

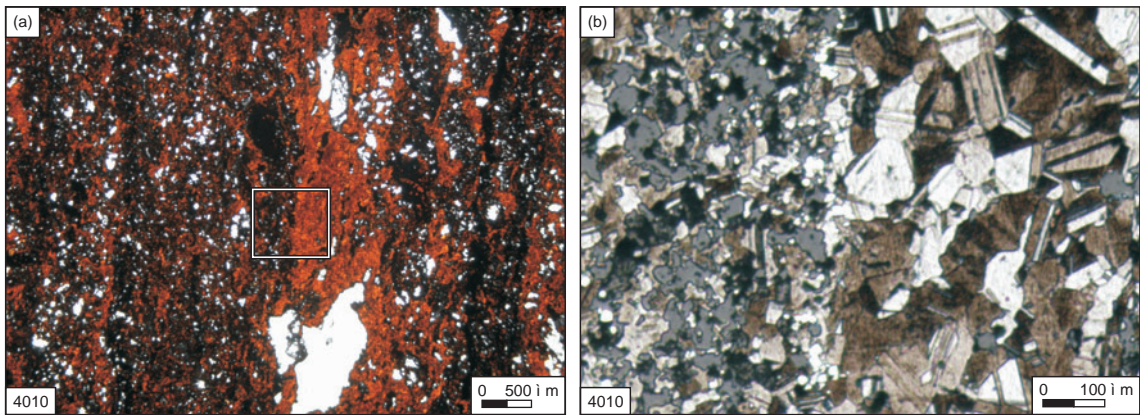


Figure 9: Two separate sphalerite grainsize domains in the fine grained sphalerite bands. Grain outlines were exposed by etching. a) Transmitted light. b) Reflected light. Sphalerite in the host rock clasts (left side) is finer than in the area where there has been dilation between originally adjacent layers in the right half of (b).

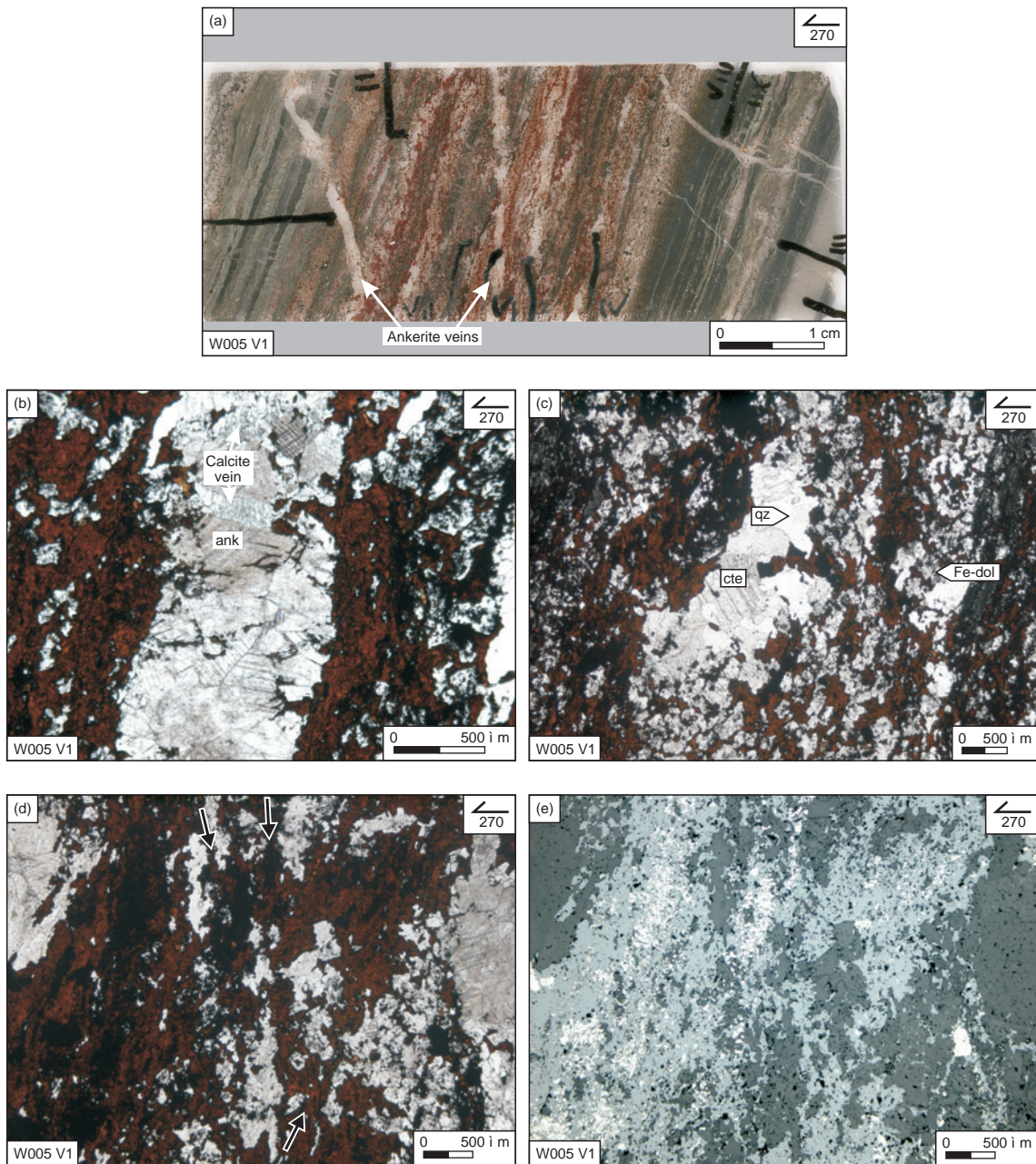


Figure 10: Fine grained sphalerite. a) Fine grained sphalerite band containing steeply east-dipping ankerite veins. Thinsection photograph, vertical section. b) Ankerite vein in (a) cut by a calcite-quartz vein (see also Fig. 11) with sphalerite deposited along the grain boundaries of both generations of carbonate. Vertical section, transmitted light photomicrograph. c) The matrix in the fine grained sphalerite bands comprises fine grained ferroan dolomite and coarser calcite and quartz. Sphalerite is deposited along grain boundaries indicating later timing than ferroan dolomite and calcite-quartz alteration. Arrows indicate east-dipping trend of sulphide aggregates. Vertical section, transmitted light photomicrograph. d and e) Fine grained sphalerite band with microcrystalline pyrite inclusions in host rock clasts (dark areas) contained within sphalerite patches particularly notable in the large patch in the left half of the image. Vertical sections, transmitted light (d) and reflected light (e) photomicrographs.

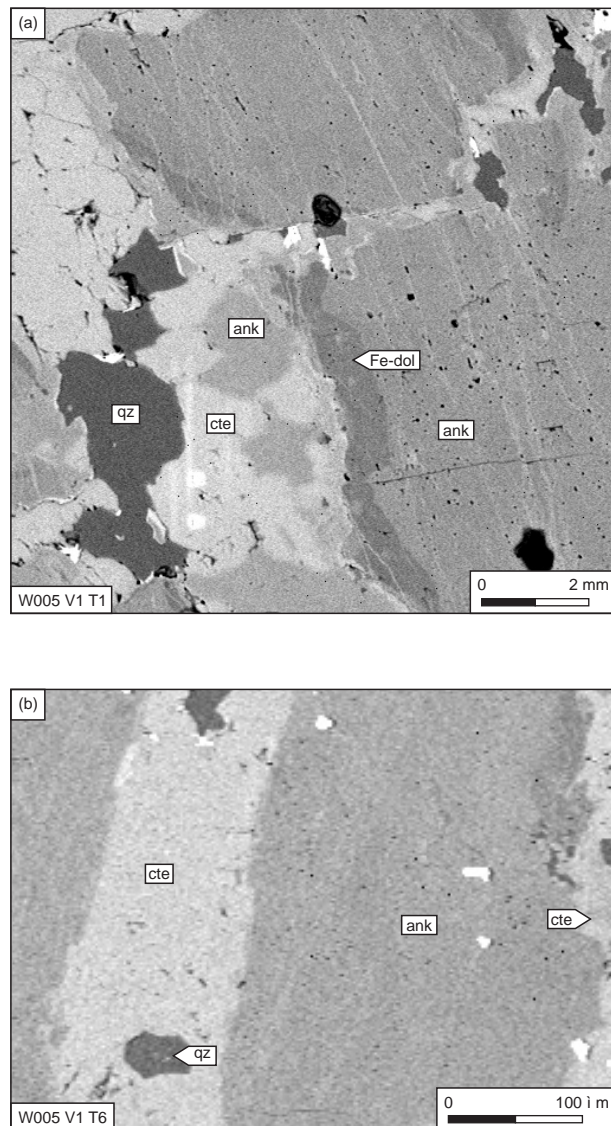


Figure 11: Backscatter images of carbonate alteration. a) Ankerite, from the matrix of a fine grained sphaerite breccia, is cut by a quartz calcite vein with a ferroan dolomite selvage and inclusions of ankerite indicating replacement occurred at this scale. The fine white streaks through the ankerite are calcite as well. b) Fibrous calcite and quartz vein cutting ankerite vein in figure 10b.

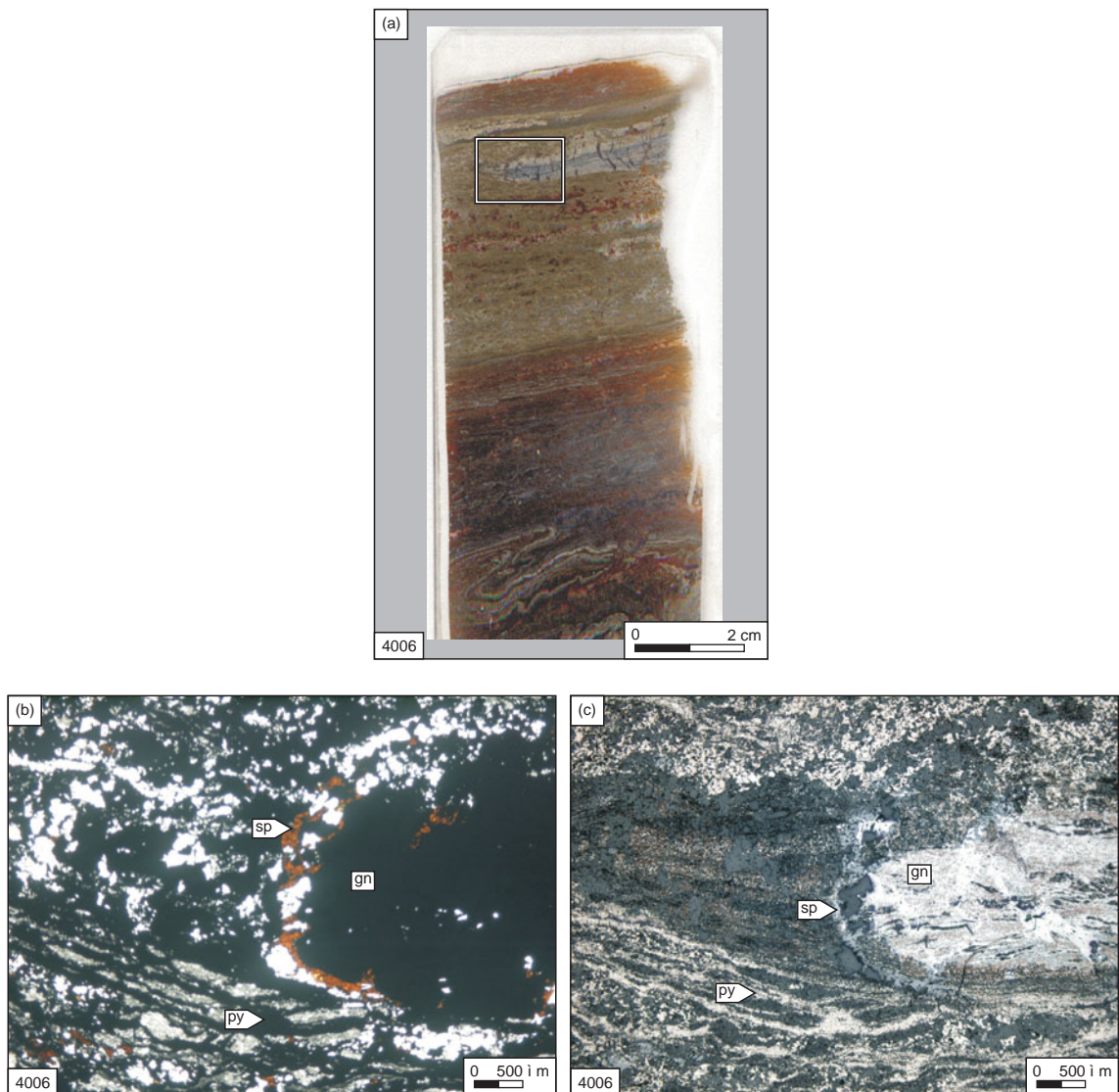


Figure 12: Alteration front at the edge of a rare galena band. a) Thinsection of microcrystalline pyrite band containing a band of galena. b) Large opaque patch is the edge of a galena with a halo of sphalerite. Microcrystalline pyrite forms anastomosing opaque seams. Transmitted light photomicrograph. c) The lobe of galena contains inclusions of microcrystalline pyrite in patches that extend beyond the galena and sphalerite alteration. The fabric of the rock revealed by microcrystalline pyrite is the same in the galena bands and in surrounding areas. Reflected light photomicrograph.

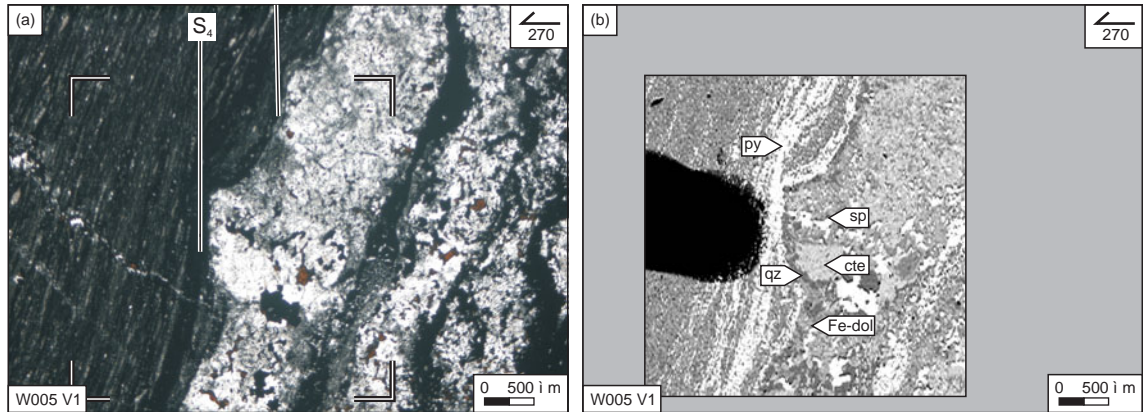
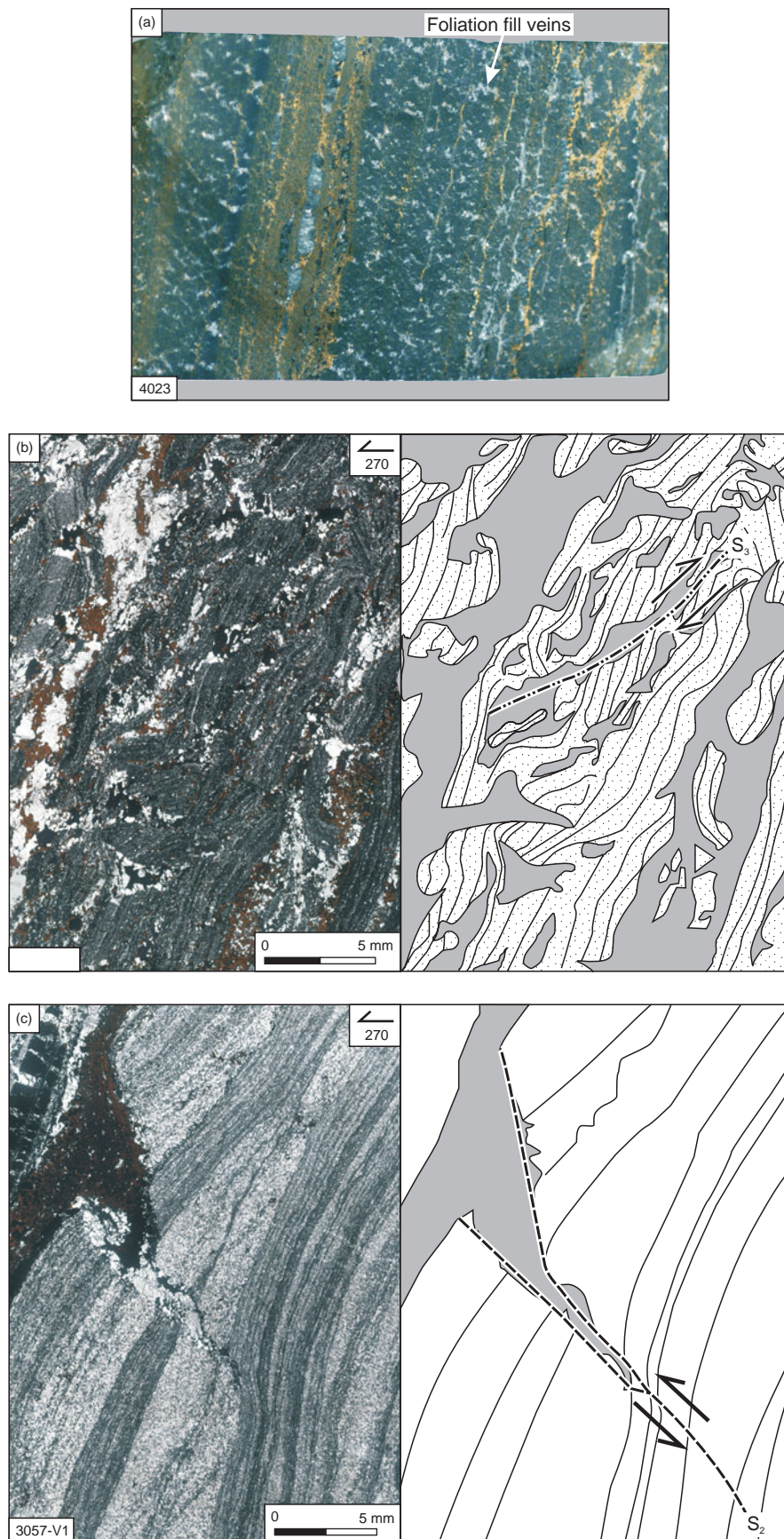


Figure 13: Porphyroblastic carbonate layer containing sphalerite and pyrrhotite. a) So-called nodules situated between S₄ crenulation cleavages in the surrounding carbonaceous shales. Vertical section, reflected light photomicrograph. b) Backscattered image of area indicated in (a) showing quartz, calcite and sphalerite overprinting ferroan dolomite in the porphyroblast part of the layer.



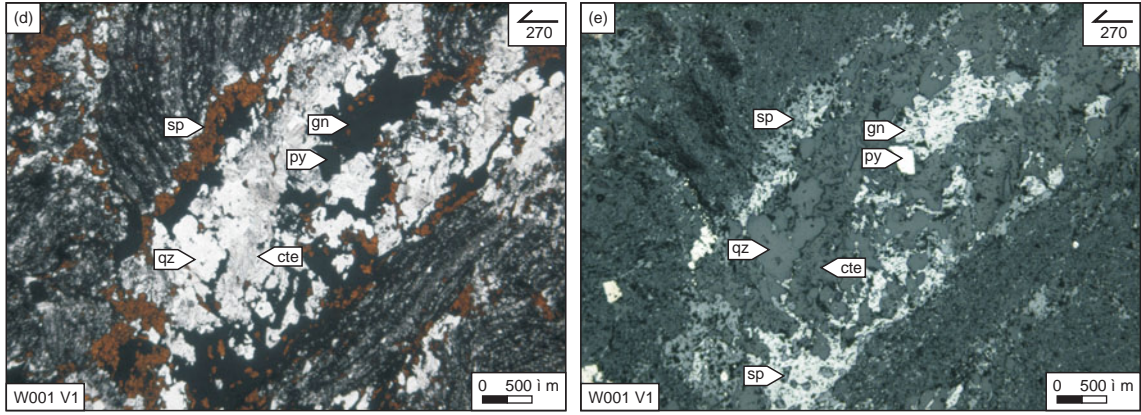
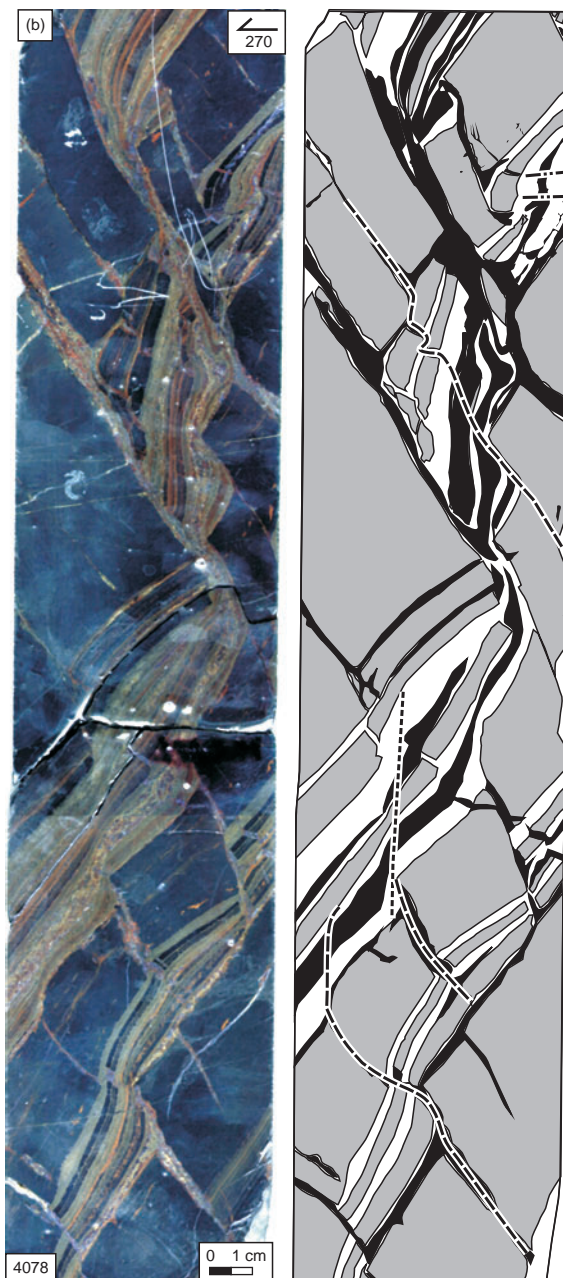
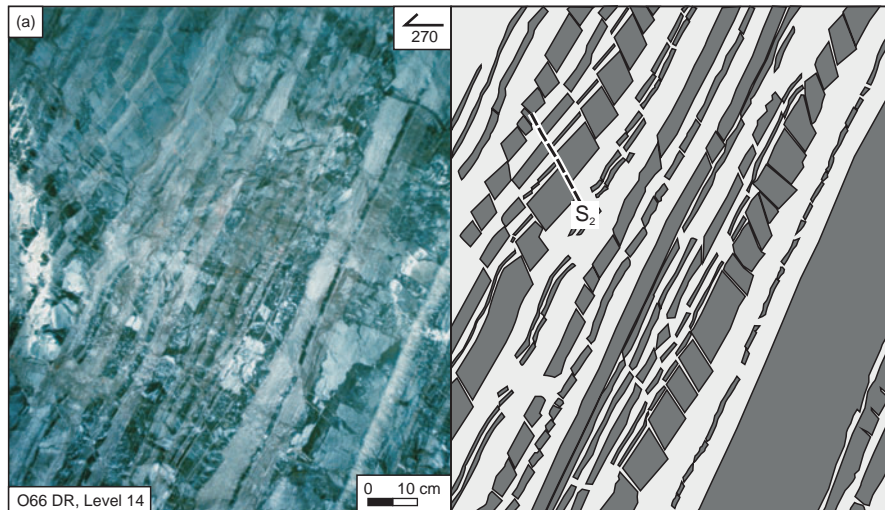


Figure 14: Foliation fill breccias. a) Drill core sample of foliation fill breccia. Foliation fill veins trend mainly to the lower right. Left of centre is a quartz-calcite vein with sphalerite selvage. b) Foliation fill breccia in laminated carbonaceous shale. The west-dipping veins are discordant to bedding where they coincide with S_3 crenulation cleavages and parallel to bedding where the vein crosses between adjacent cleavage seams. Photomicrograph and sketch c) Detail of dilated and sulphide filled crenulation cleavage. The width of the vein is related to the difference between the orientation of the opposite sides, indicating that the rotation of the wall rock on one side relative to the other caused dilation of the host structure. Vertical section, transmitted light photomicrograph. d and e) Foliation fill veins, transmitted light (ppl) and reflected light respectively. The overprinting sequence in the fill is quartz and calcite followed by sphalerite and then galena and lastly pyrite.



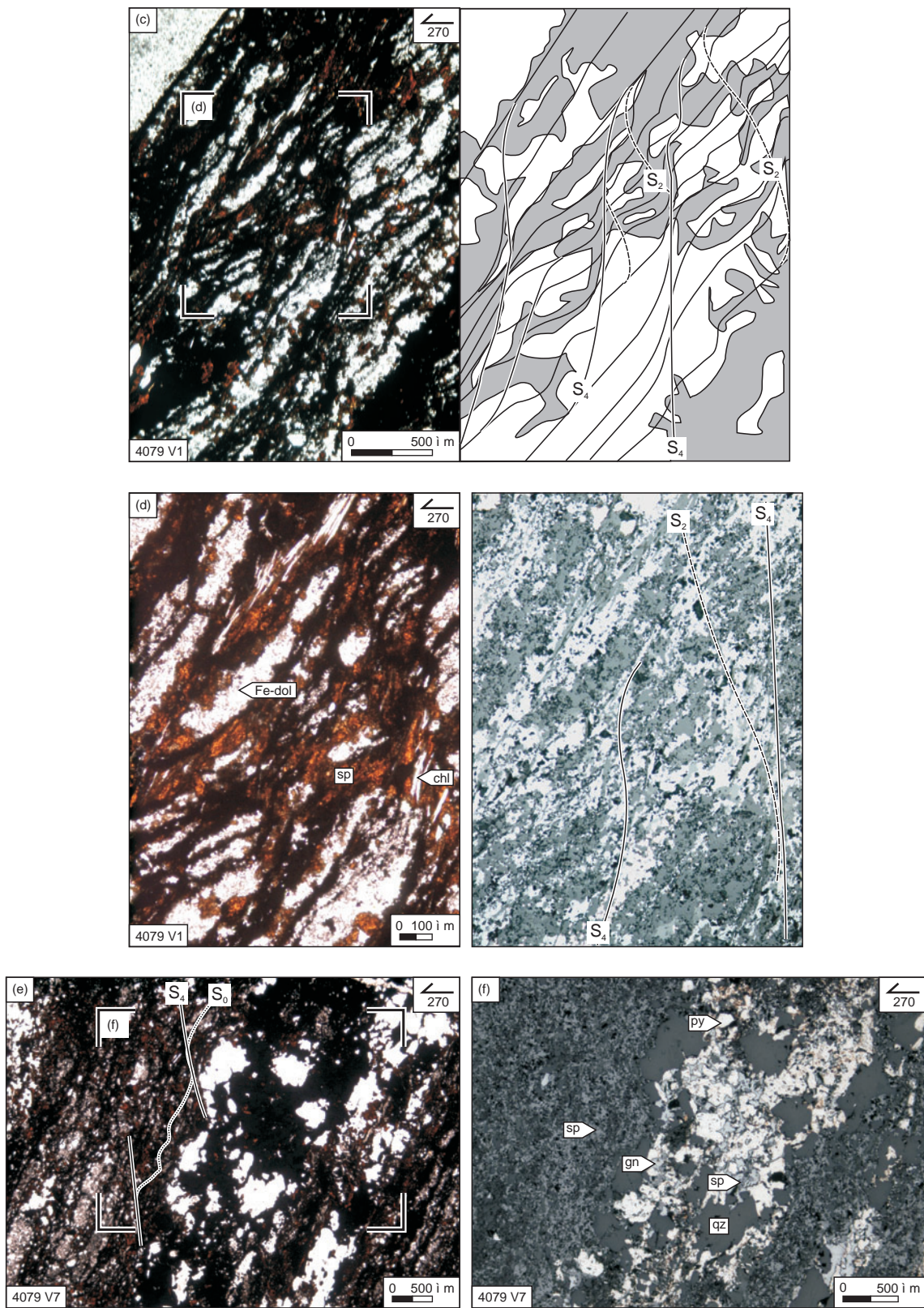


Figure 15: Asymmetric boudin breccias. a) Underground exposure of asymmetric boudin breccia. b) Interboudin planes are disjunctive S_2 that is locally rotated in to vertical S_4 , which has east block up apparent displacement. Black areas in the sketch show the location of sphalerite and associated alteration. Sulphide has replaced the host rock carbonaceous shale and infill carbonate cleavages and bedding plane partings that have dilated. c) Transmitted light photomicrograph left and sketch right. d) Transmitted light and reflected light photomicrographs, left and right respectively. e and f) Infill between laying. Infill material comprises qz-cte-sp-gn-py (see also Figs 8, 10 and 14). Transmitted light (left) and reflected light (right) photomicrographs. Location of (f) is illustrated in (e).

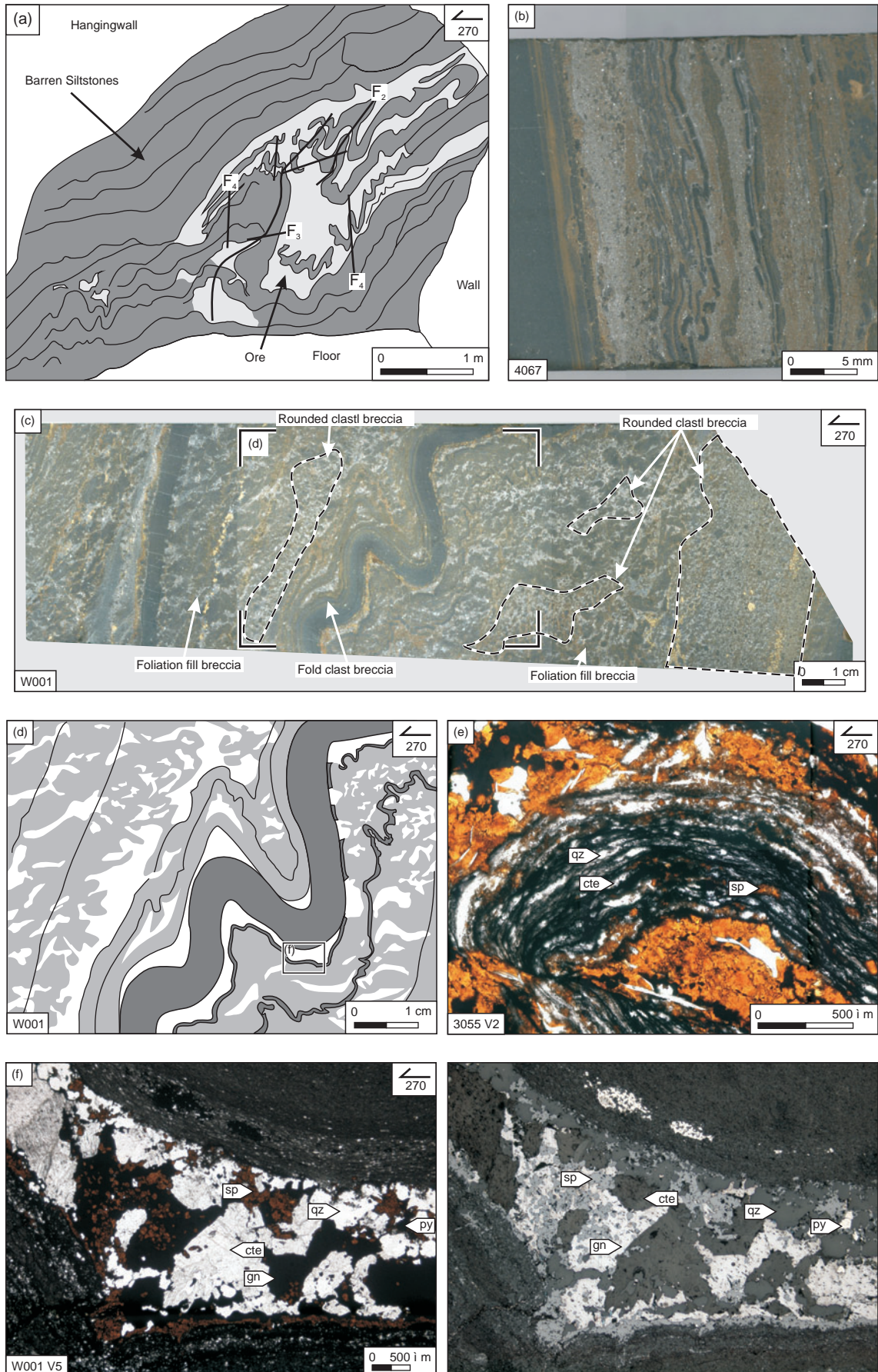


Figure 16: Fold Clast breccias. a) Underground exposure of fold clast breccias (14CA, 6527 mN, 2445 mRL). b) Millimetre scale fold clast breccia in drill core. c) Hand specimen of breccia containing all three breccias patterns. Vertical section. d) Sketch of fold clast breccia in (c). Alteration is contained between layering in the hinges of folds, and on some limbs between. e) Photomicrograph of a clast of folded carbonaceous shale containing quartz, calcite and sphalerite replacing the deformed layer. f) Infill between layering in a fold hinge that comprises calcite and quartz with minor ferroan dolomite overprinted by sphalerite and then galena which replace carbonate. Inclusions of sphalerite in galena indicate the later relative timing of the latter sulphide. Transmitted light (left) and reflected light (right) photomicrographs, vertical sections, location shown in (d).

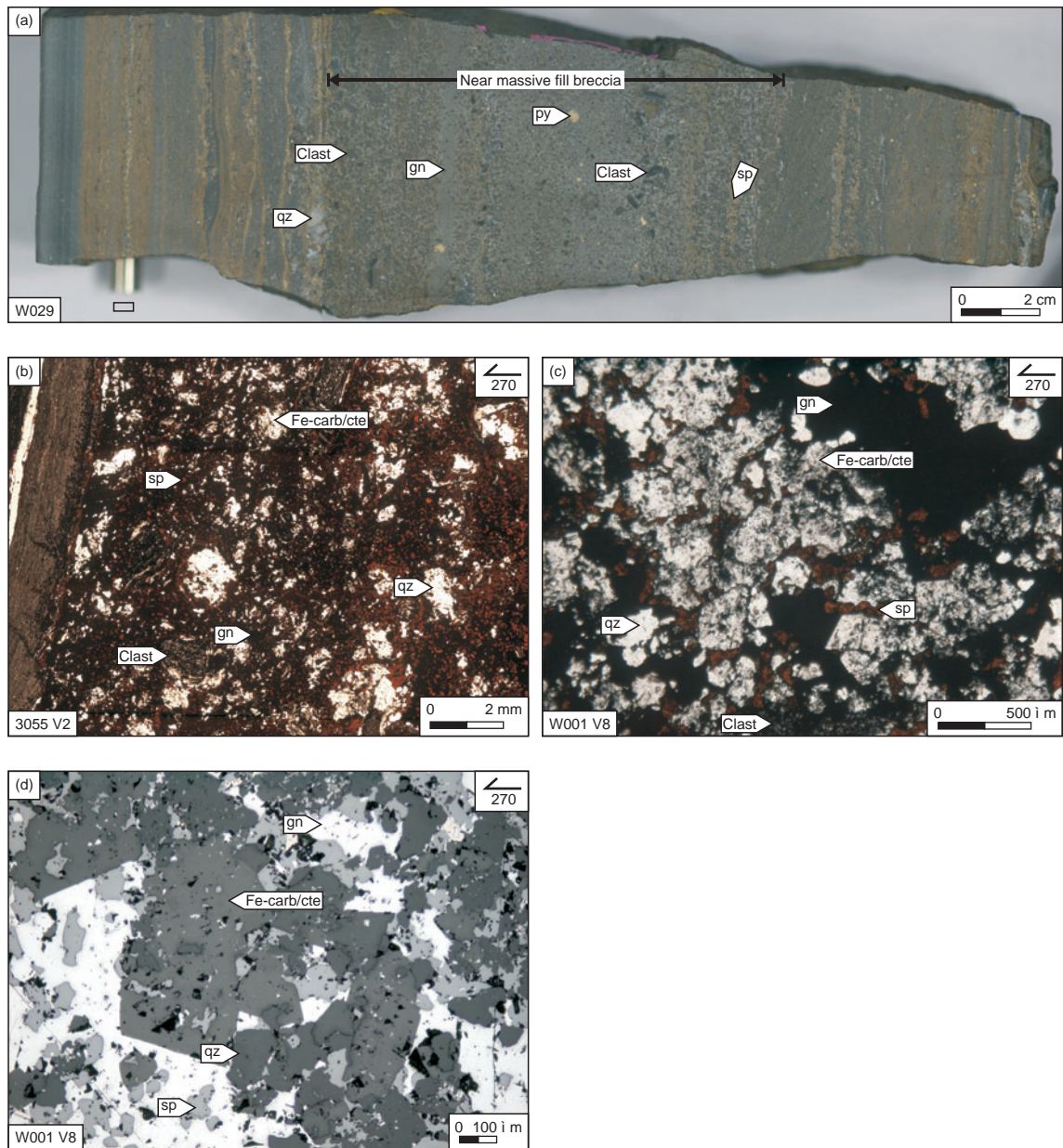


Figure 17: Rounded clast breccia. a) Hand specimen. Speckled appearance is due to fine clasts of carbonaceous shale. b) Photomicrograph collage of breccia. This sample is located between unfolded wall rocks (right side) and fold clast breccia (left out of view; see also Fig. 25b). Foliated clast of carbonaceous shale are situated in a matrix of carbonate (a mixture of calcite and ferroan dolomite), quartz and sulphides. Vertical section, transmitted light. c) Sulphide alteration in the matrix of near massive fill breccia. Vertical section, transmitted light. d) Breccia matrix with sphalerite situated along quartz and carbonate grain boundaries and as inclusions in galena. Textures indicate quartz and carbonate are overprinted by sphalerite and galena.

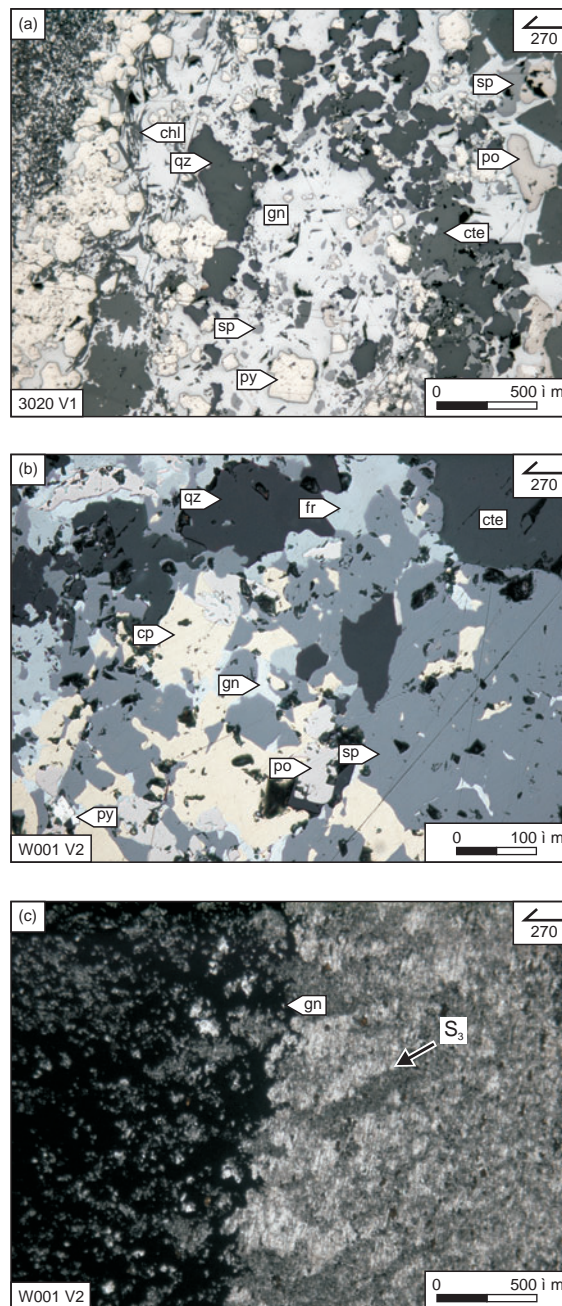


Figure 18: Ore sulphide overprinting relationships. a) The first sulphides deposited were sphalerite and pyrrhotite, which are inclusions in the dominant galena, in which quartz, calcite and chlorite are also inclusion phases. Reflected light photomicrograph. b) Coexisting sphalerite, pyrrhotite, galena chalcopyrite, freibergite and pyrite. The oldest sulphides are sphalerite and pyrrhotite which have embayed margins where freibergite, galena and chalcopyrite have replaced them. c) Galena replacing carbonate. Galena overprints patches of fibrous carbonate that elongated in the direction of S_3 with vertical fibres indicating the D_4 extension direction.

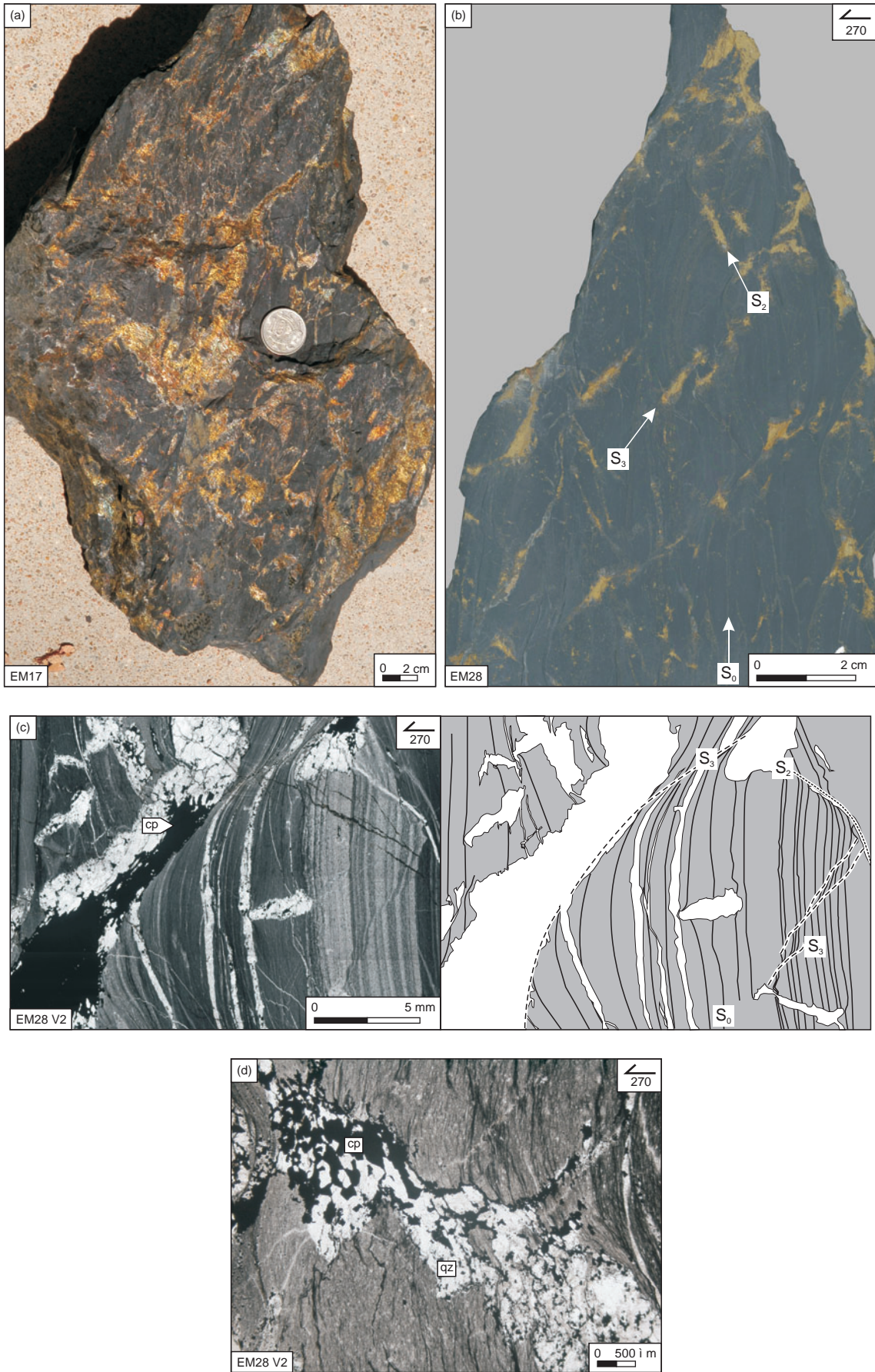


Figure 19: Breccias that comprise the copper orebodies in the Enterprise mine. a) Irregularly shaped chalcopyrite and pyrrhotite patches on a broken surface, as they typically appear in underground exposures. b) Vertical section showing the regular distribution of sulphides in east- or west dipping aggregates. c) Sulphide aggregates are located in ferroan dolomite and quartz veins hosted in east- or west dipping shear bands and at the intersection of these structures. The orientations and displacements of these shear bands is consistent with S_2 and S_3 . Vertical sections. d) Chalcopyrite is located filling grains, along grain boundaries and in fractures in foliation hosted quartz veins. Transmitted light photomicrograph, vertical section.

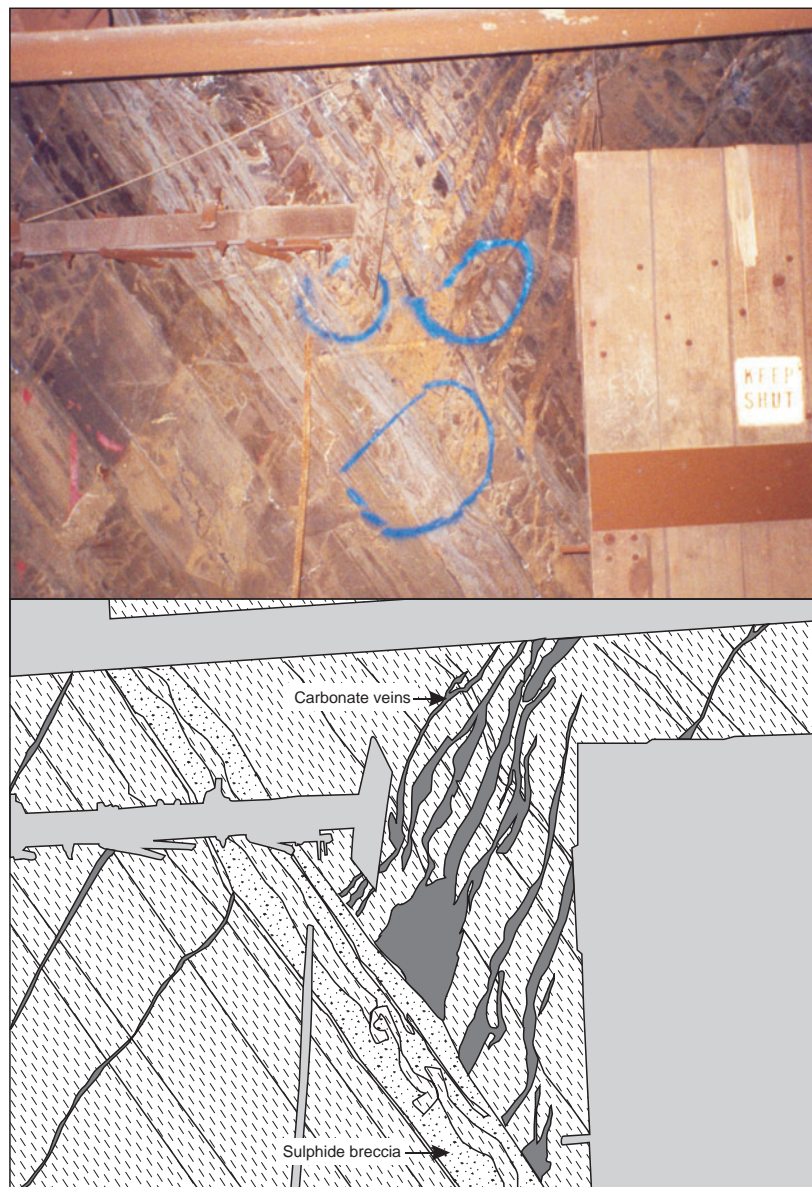


Figure 20: Underground exposure of east-dipping carbonate veins on the margins of a sulphide breccia. Looking south (Level 5, T62 N DR near tipple).

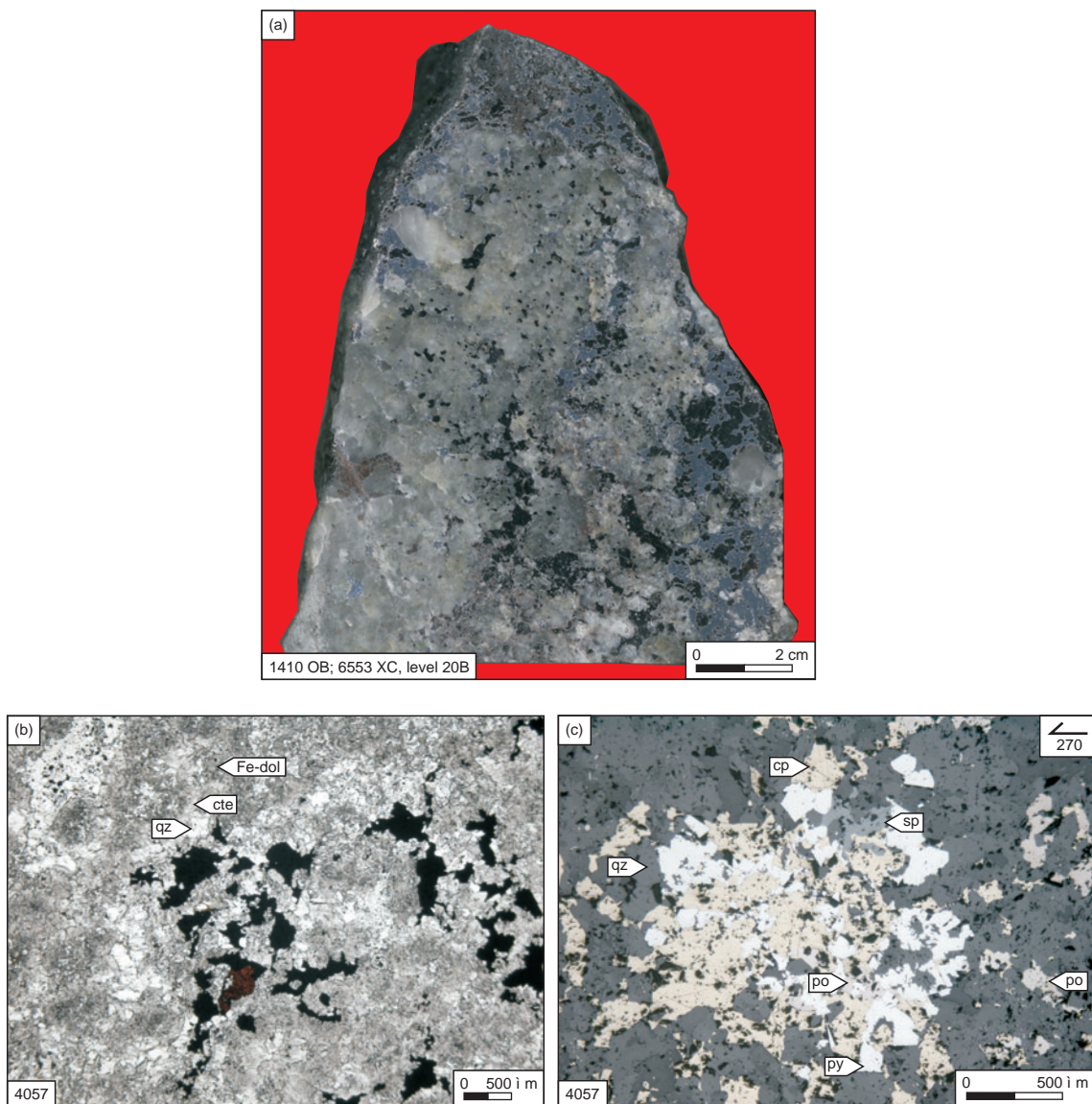


Figure 21: Samples from the stratiform transitional silica-dolomite zone between the copper and Zn-Pb-Ag orebodies. a) Hand specimen containing galena and sphalerite interstitial to quartz and replacing dolomite and calcite. Rounded sphalerite cores surrounded by galena show it was the first of these base metal sulphides to be deposited. b) Photomicrograph of transitional silica-dolomite alteration. The mottled appearance in the non-sulphide part of the rock is caused by calcite and quartz alteration of the ferroan dolomite host rock which is grey compared to the alteration minerals. The sulphides (chalcopyrite and sphalerite) are interstitial to calcite and quartz. Transmitted and plane polarised light. c) Photomicrograph of a patch containing chalcopyrite, pyrite, pyrrhotite and sphalerite in stratiform silica-dolomite alteration between the copper and Zn-Pb-Ag orebodies.

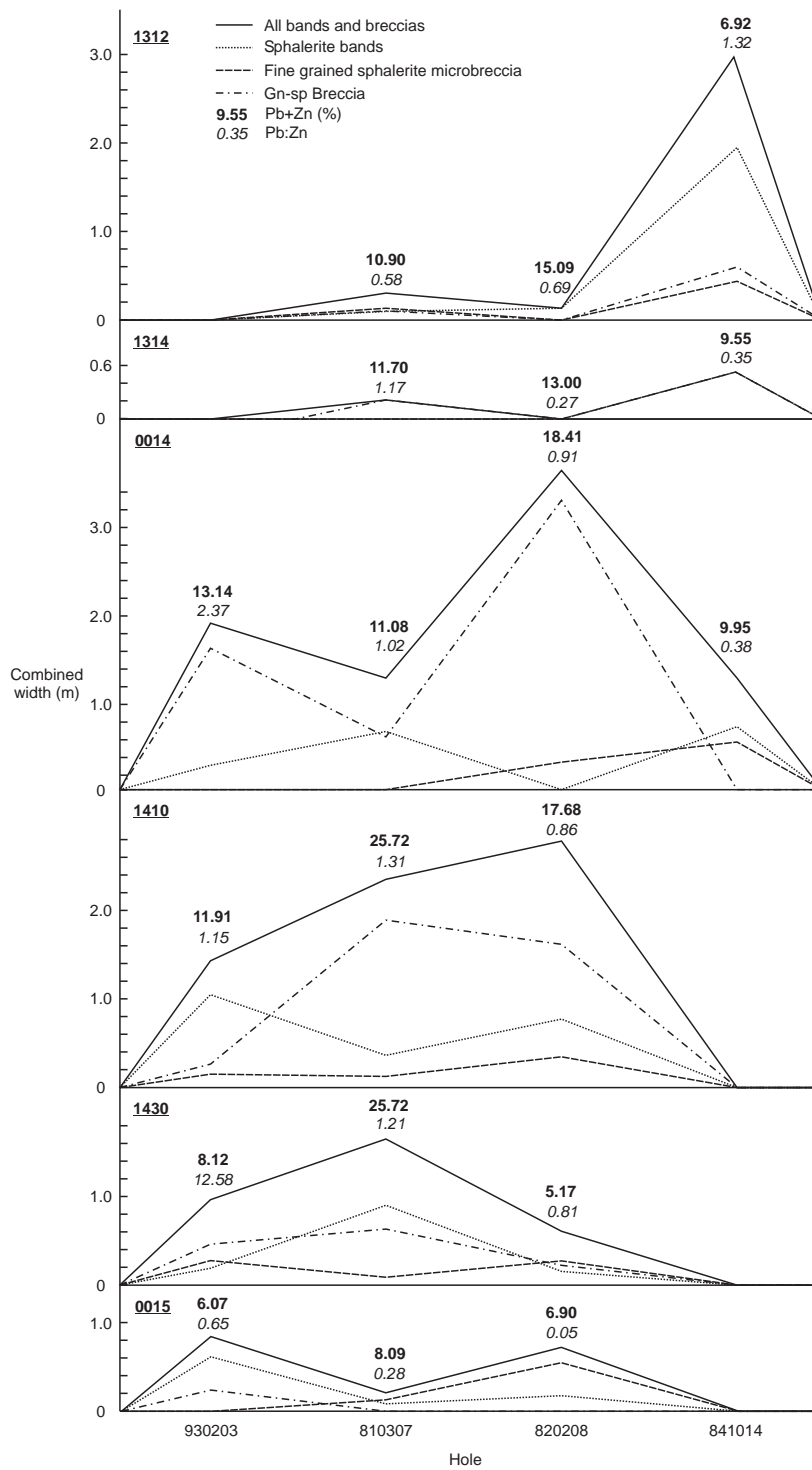
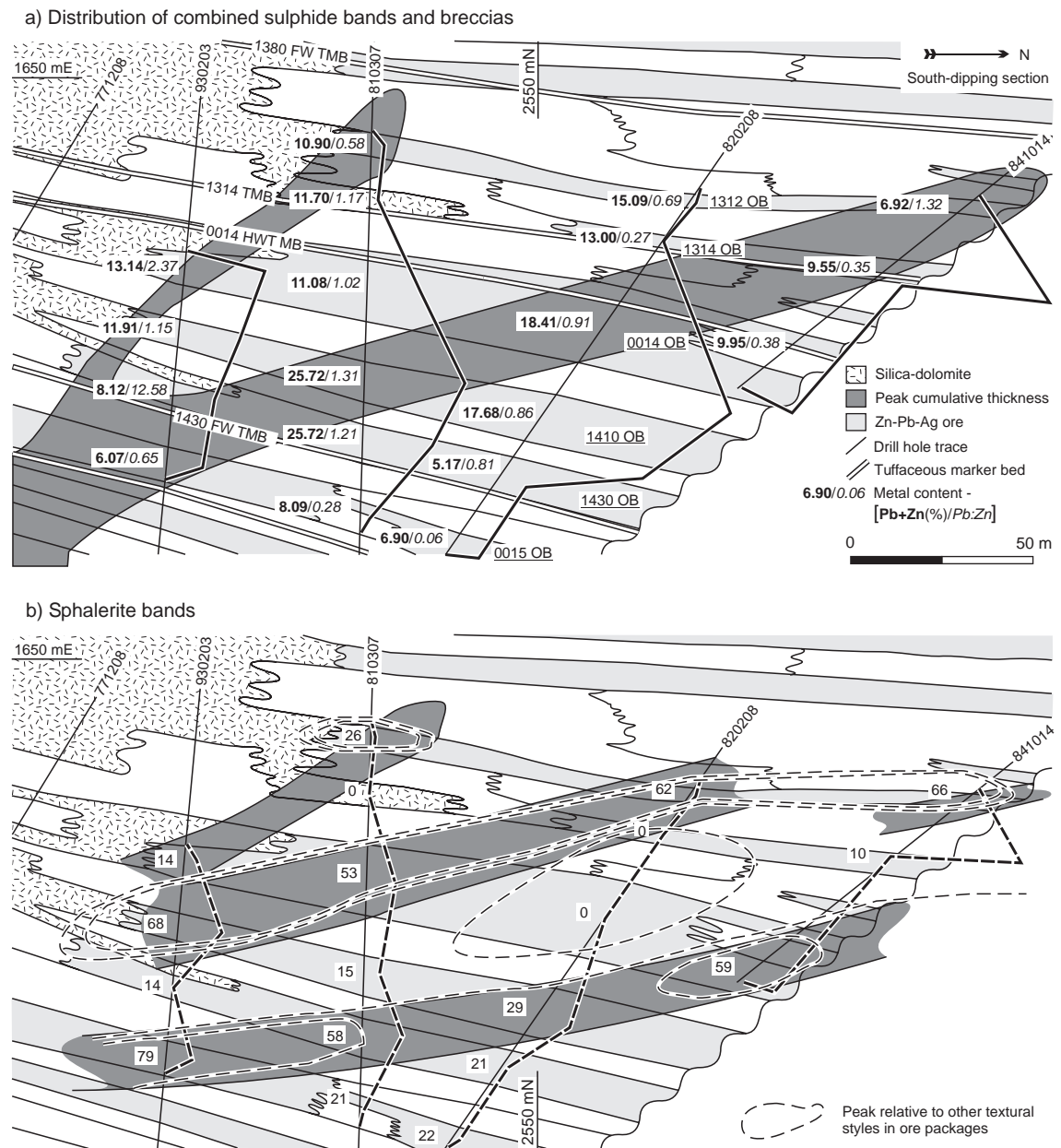


Figure 22: Graph illustrating the cumulative thickness of textural styles in each ore package in Lens K and 0015 which is the ore package immediately east of Lens K. Graphs are stacked in sequence from top to bottom starting with the western most package (1312). Drill holes are arranged left to right from south to north. Figures above the graphs are Pb+Zn % (bold) and Pb:Zn (italicised) for the intersection through each ore package. There is a general decrease in Pb:Zn to the north.



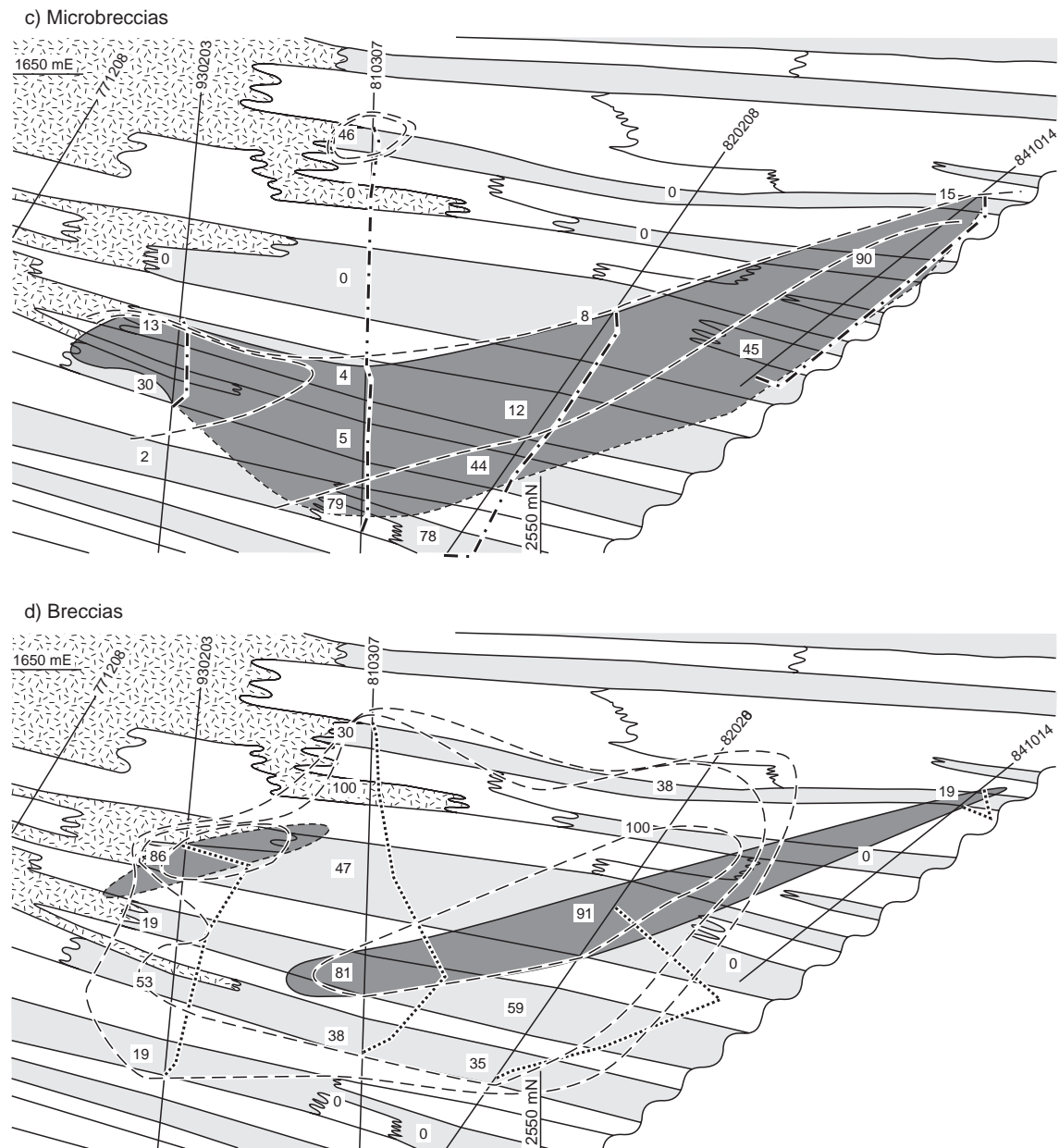


Figure 23: Plans showing the distribution of the main textural groupings. Graphs in figure 21 are transferred to the corresponding drill holes, with the y-axis perpendicular to the hole trace. Dark areas are peaks of cumulative thickness. The percentage of the textural style in the intersected ore package is denoted by figures next to drill hole traces and the peaks are delineated. a) Combined thickness of all bands and breccias. The distribution contains NNW-SSE-striking peak and a more NW-SE striking one ahead of the silica-dolomite alteration front. b) Sphalerite bands (microcrystalline and fine grained styles excluding microbreccias) display two NNW-SSE-striking peaks that straddle the peak in (a). A third peak is located north of the silica-dolomite alteration front is coincidental with a similar peak in (a). Cumulative thickness and percentage peaks of the textural style in the ore package are coincidental. c) Fine grained sphalerite microbreccias have a single NNW-SSE-striking peak thickness that overlaps with the total band and breccia peak in (a). d) Breccias have a NNW-SSE-striking cumulative thickness peak coincidental with the total peak in (a) and a peak area north of the silica-dolomite alteration front. The percentage contours are widely spread of but have a NNW-SSE-striking high in the centre.

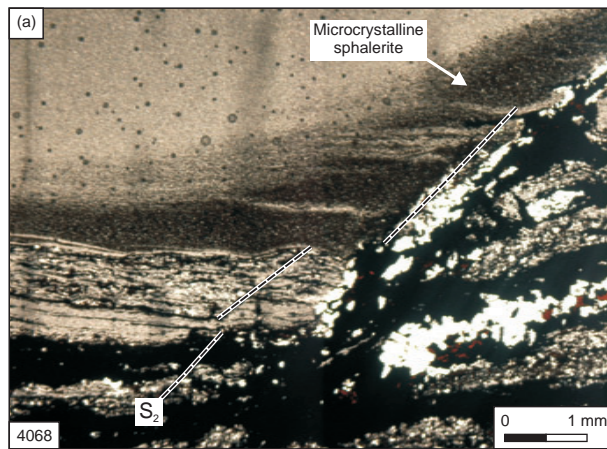
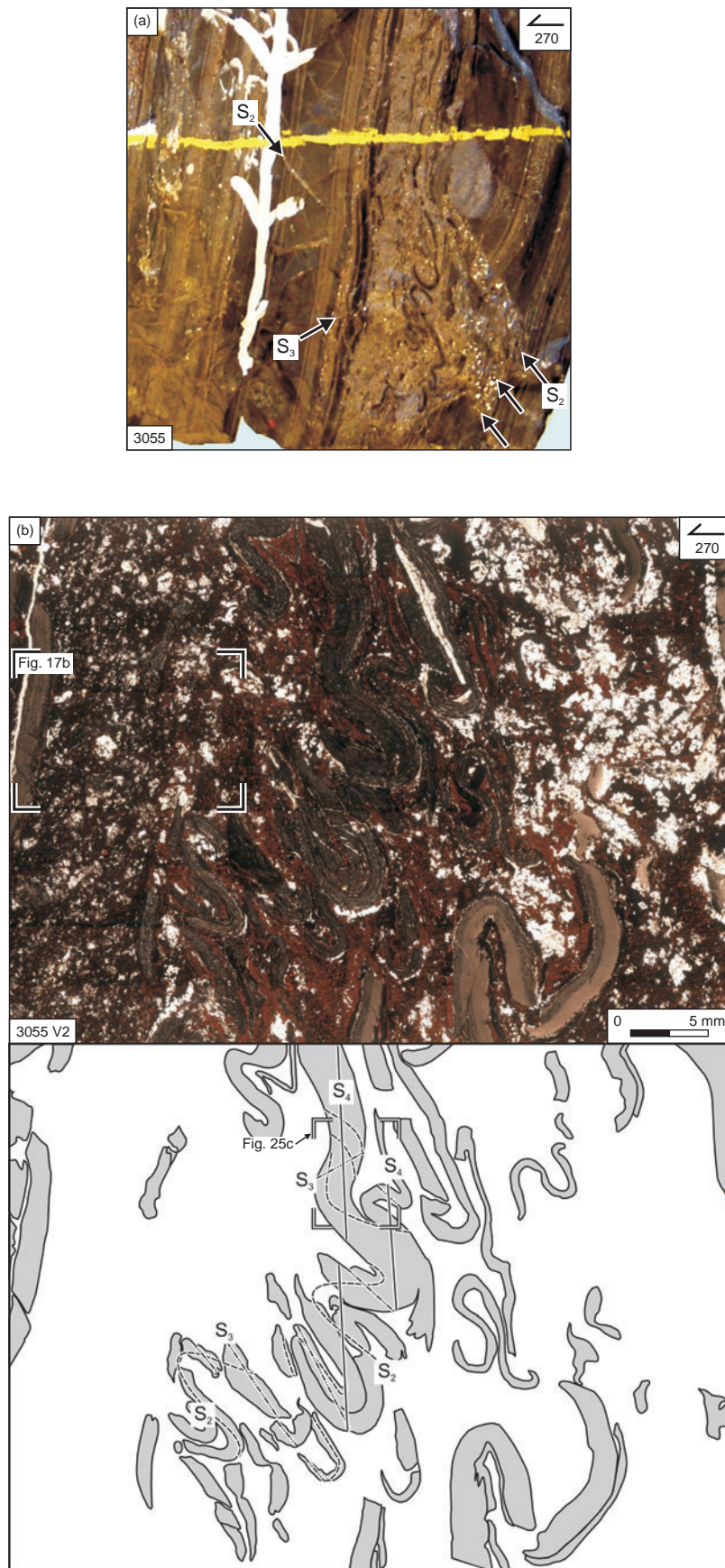


Figure 24: Microcrystalline sphalerite alteration front extending from an S₂ hosted vein. Vein comprises qz-cte-sp-gn-cp±po±py. Transmitted light photomicrograph.



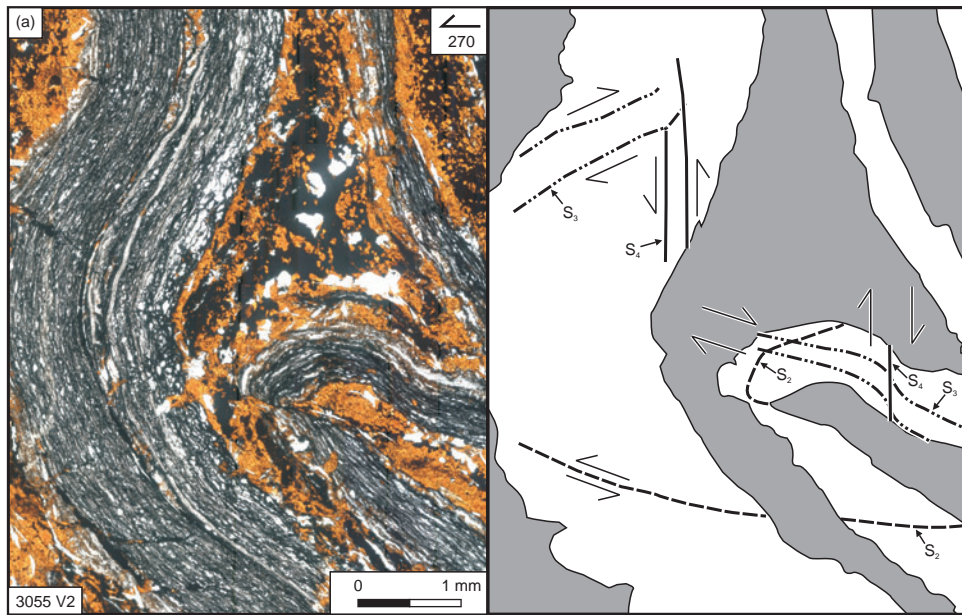


Figure 25: Structural features of fold clast breccias. a) Hand specimen with the breccia localised along strike of east-dipping disjunctive S_2 cleavages in the adjacent siltstones. Folding of layering in brecciated interval decreases away from the disjunctive cleavage. Vertical face, looking north. b) Photomicrograph collage and trace (below) of the breccia in (a). Broken lines show the cleavage relationships. c) Disharmonic fold clast analysed in detail in figures 26 and 27, location is indicated in (b) (see text for detail). Vertical sections, transmitted light.

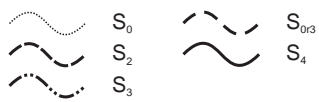
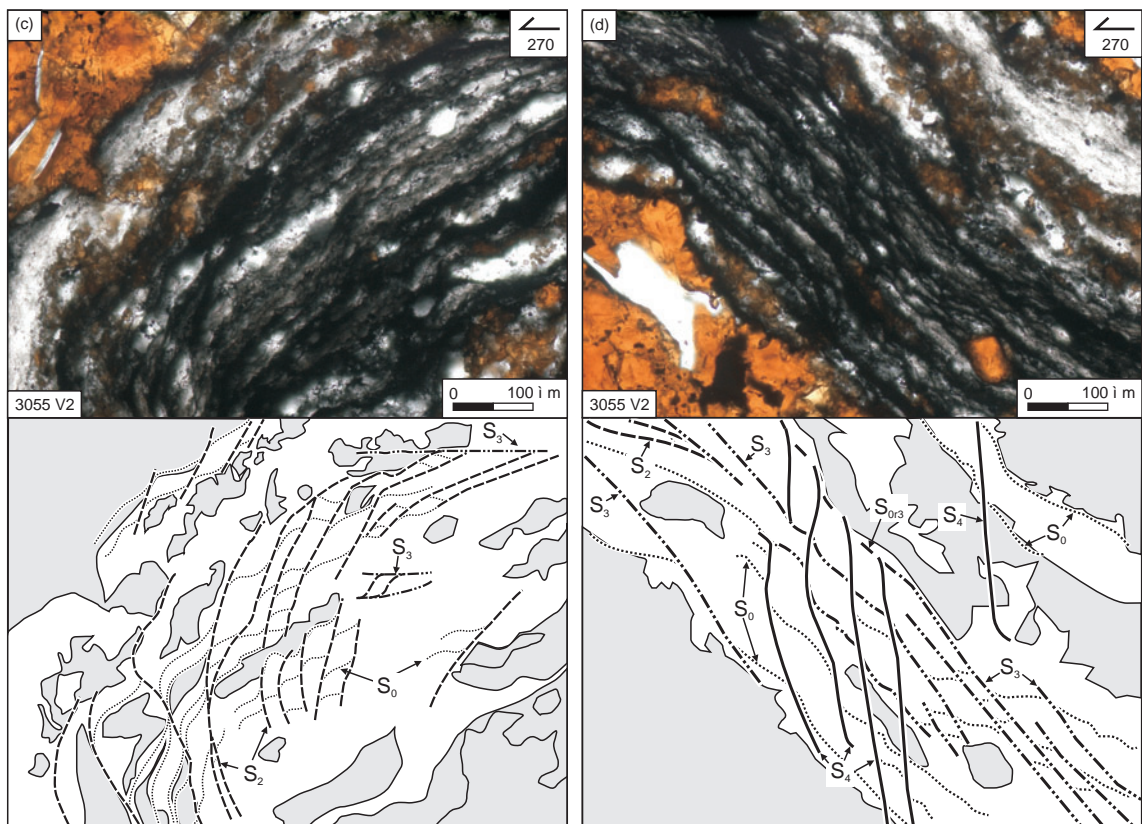
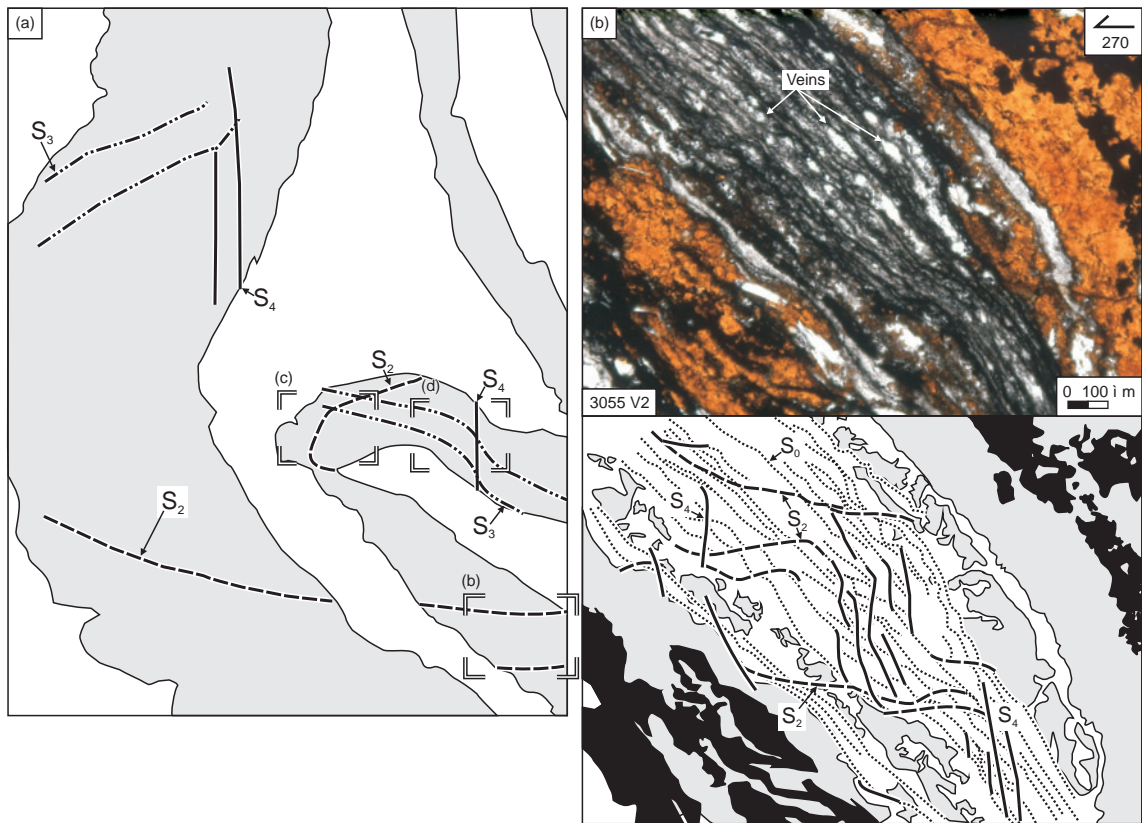


Figure 26: Detailed cleavage relationships of the tightly folded layer in figure 25c (vertical sections). a) Location of b, c and d. b) Long limb, S_2 is shallow dipping with top to the west displacement, S_4 is vertical and has east block down shear sense and there is a paucity of S_3 . c) Hinge. S_2 is folded by S_3 which has horizontal with top to the east shear sense and is also axial planar to the fold. d) Short limb, S_3 is folded by S_4 , which is vertical and has east block down shear sense.

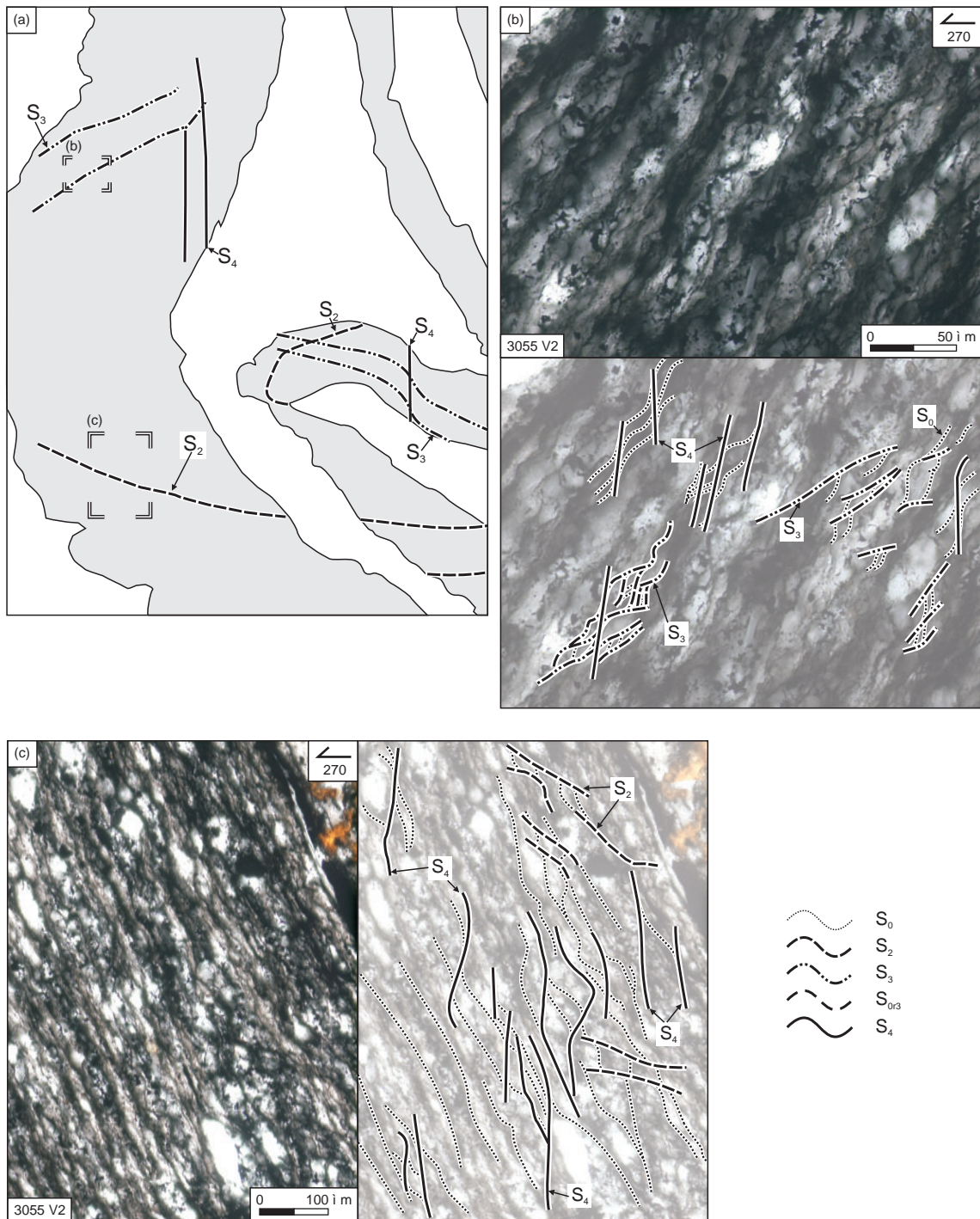


Figure 27: Detailed Cleavage relationships of the gently folded layer in figure 25c. b) The short limb contains vertical S_4 with east block up shear sense. S_3 is west-dipping with top to the east movement and S_2 is steep. c) The long limb has vertical S_4 with east block down shear sense, shallow east-dipping S_2 with top to the west shear sense and a paucity of S_3 , is the same as the long limb in the tightly folded layer

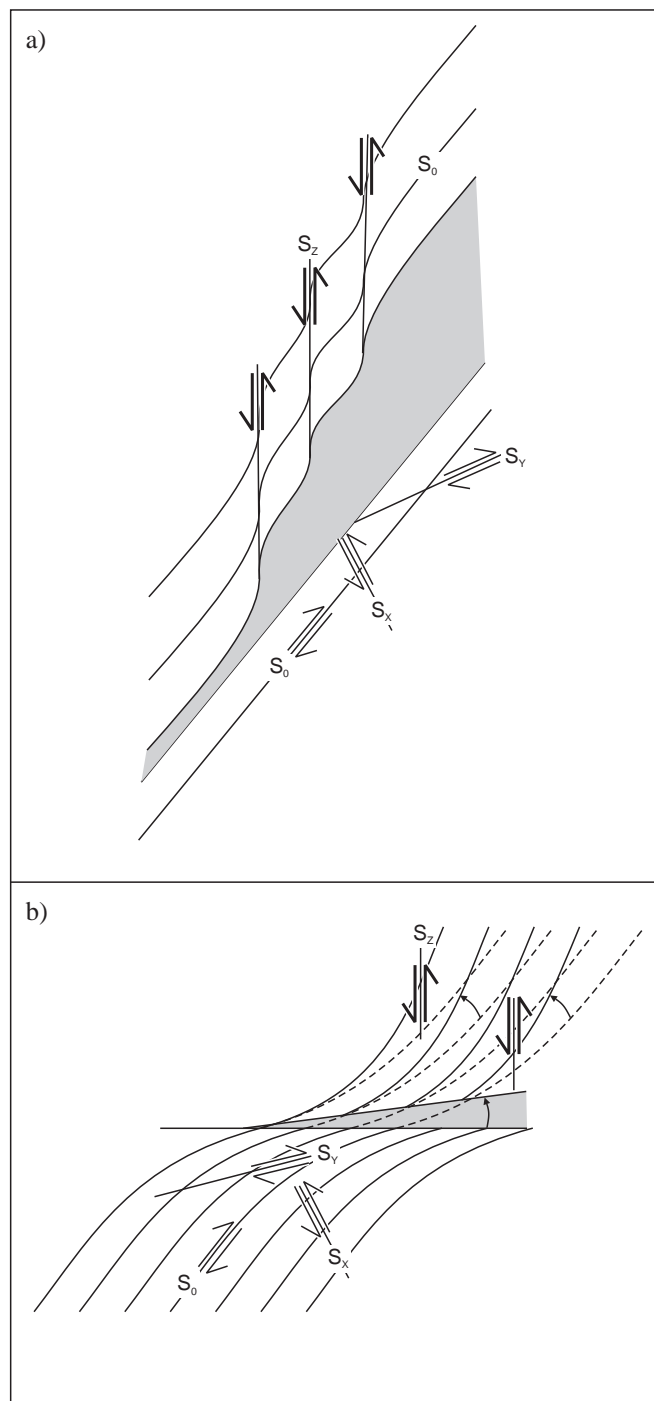


Figure 28: Schematic illustration of planar vein formation. a) Veining along bedding and b) along a discordant foliation. In both cases the upper block is rotated anticlockwise by right block up shear sense along S_z . In the lower blocks shearing strain is either along older foliations or lower strain along S_z . Alphabetic subscripts are used to emphasise that any generation of structure can be involved in the deformation causing dilation.

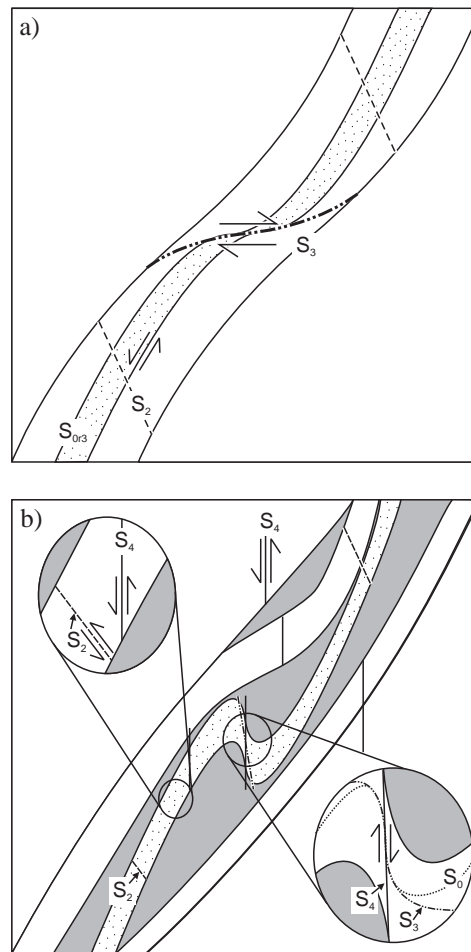


Figure 29: Schematic illustration of disharmonic folding and dilation in the fold clast breccias. a) A horizontal D_3 shear band localised within thin bedded units sandwiched between thick bedded siltstones. Reactivation of S_2 outside of the shear band. Vertical section looking north. b) Final stage of disharmonic folding, which included dilation. The short limb of the tightly folded layer experiences right block down shearing. Whereas the opposite shear sense prevails throughout the gently folded layers. Reactivation of S_2 causes dilation along the long limbs. See also figure 24.